INTERNATIONAL JOURNAL OF CLIMATOLOGY
Int. J. Climatol. **30**: 2175–2194 (2010)
Published online 16 October 2009 in Wiley Online Library
(wileyonlinelibrary.com) DOI: 10.1002/joc.2039

RMetS
Royal Meteorological Society

Atmospheric moisture budget in the Arctic based on the ERA-40 reanalysis

Erko Jakobson[a]* and Timo Vihma[b]
[a] *Institute of Environmental Physics, University of Tartu, Tartu, Estonia*
[b] *Finnish Meteorological Institute, Helsinki, Finland*

ABSTRACT: The atmospheric moisture budget in the Arctic in 1979–2001 was analysed on the basis of the ERA-40 reanalysis. Zonal variations in the profiles of specific humidity mainly occur at altitudes below 5 km. The moisture transport peaks at altitudes lower than previously suggested; the median peak level of meridional moisture flux (MMF) across 70°N is in winter at 930 hPa pressure level and in other seasons at 970–990 hPa level. Mean precipitable water for the polar cap (70–90°N) ranges from 2.4 mm in winter to 12.3 mm in summer. Transient eddies (TE) are responsible for most of the water vapour transport across 70°N by providing from 81% of MMF in winter to 92% of MMF in summer. The contribution by stationary eddies (SE) ranges from 5 to 9%, whereas the contribution of mean meridional circulation (MMC) ranges from 1% in summer to 12% in winter. Relative inter-annual variation in MMF components is highest for SE (standard deviation/mean = 133%), second highest for the MMC (61%) and smallest for TE (4%). The MMF across 70°N accounts for 59% of the annual precipitation. Averaged for the polar cap, the mean annual moisture flux convergence (192 mm) and net precipitation (179 mm) are close to each other, but local differences exceeding 200 mm occur at several places. Over the open ocean, the moisture flux convergence is considered more reliable. The Arctic Oscillation (AO) index correlates with MMF in spring and winter (correlation coefficient $r = 0.75$) and with net precipitation in spring ($r = 0.61$) and winter ($r = 0.50$). The AO and precipitable water correlate in Canada and Greenland in winter and spring ($r = -0.7$) and in Europe in winter ($r = 0.8$). Copyright © 2009 Royal Meteorological Society

KEY WORDS Arctic; ERA-40 reanalysis; water vapour; moisture flux convergence; transient eddies; stationary eddies; net precipitation

Received 3 February 2009; Revised 12 September 2009; Accepted 14 September 2009

1. Introduction

Air moisture plays an important role in several physical processes in the Arctic. Under clear skies at an air temperature of 0 °C, the downward longwave radiation at the Earth surface varies by 25 W m^{-2} depending on the amount of water vapour in the atmosphere (Prata, 1996). In the case of cloud formation, the surface radiation balance is even more strongly affected (Curry *et al*., 1996). Over the Arctic Ocean, the cloud radiative forcing at the sea surface is positive for most of the year, i.e. clouds increase the downward longwave radiation more than reducing the downward shortwave radiation (Intrieri *et al*., 2002). Cloud-top radiative cooling is a significant source of turbulence in particular over snow and ice surfaces, where convection originating from the surface is limited (Vihma *et al*., 2005). The release of condensation heat is smaller in the Arctic than at lower latitudes, but can still play an important role, for example, in the development of Polar lows (Rasmussen and Turner, 2003). Changes in the atmospheric moisture budget as well as cloud coverage and properties are key factors controlling the strength of future Arctic climate change (Sorteberg *et al*., 2007). Accurate information on the air moisture is also essential for monitoring the Arctic climate: uncertainties in the water vapour content cause errors in satellite-based observations on the surface temperature, albedo (Aoki *et al*., 1999) and sea ice concentration (Kaleschke *et al*., 2001).

Precipitation is the only significant source term for the mass balance of the Greenland ice sheet and smaller ice caps in the Arctic. Precipitation in Greenland has increased during the recent decades, but due to simultaneous increase in air and snow surface temperatures the mass balance has turned negative in most parts of the ice sheet (Box *et al*., 2006). This is the case also for several smaller glaciers in Alaska, northern Canada and Scandinavia. Precipitation also affects the mass balance of sea ice, both directly via snow ice formation due to ocean flooding and superimposed ice formation due to refreezing of melt water (Granskog *et al*., 2006) and indirectly by controlling variations in the snow/ice surface albedo (Cheng *et al*., 2008).

In contrast to most of the World Ocean, in the Arctic Ocean the stratification is primarily controlled by salinity instead of temperature. The salinity distribution is controlled by the net precipitation, river discharge,

* Correspondence to: Erko Jakobson, Institute of Environmental Physics, University of Tartu, Tartu, Estonia.
E-mail: erko.jakobson@ut.ee

advection and mixing in the ocean, as well as sea ice formation and melt. The net precipitation directly contributes to 24% of the annual mean freshwater input to the Arctic Ocean, whereas river discharge contributes 38% (being itself controlled by the net precipitation over the catchments areas) and inflow through Bering Strait 30% (Serreze *et al*., 2006). Except parts of the Norwegian and Barents Seas, net precipitation is positive in the sea areas north of 50°N (Kållberg *et al*., 2005). A positive net precipitation lowers the surface salinity, strengthens the stratification, helps sea ice formation and tends to decrease deep water formation, e.g. in the Greenland Sea and Labrador Sea (Dickson *et al*., 1996). The freshwater in the Arctic Ocean has a residence time of about a decade, whereas that for water vapour in the Arctic atmosphere is about a week (Serreze *et al*., 2006).

In the ice/snow-covered parts of the Arctic, evaporation is typically small and there are no significant local sources of water vapour. Hence, precipitation is dependent on the atmospheric moisture transport from lower latitudes. Estimates of the total moisture transport into the Arctic have been made on the basis of surface observations on precipitation and evaporation (Sellers, 1965), radiosonde soundings (Peixoto and Oort, 1983, 1992; Overland and Turet, 1994; Serreze *et al*., 1995a, 1995b; Serreze and Barry, 2000; Gober *et al*., 2003), satellite data (Groves and Francis, 2002) and atmospheric reanalyses (see below). Scatter between these results is large. Estimates based on reanalysis are usually higher than those based solely on rawinsonde data, because the rawinsonde network is insufficient to capture all moisture pathways to the polar cap (Serreze *et al*., 2006). The pole-ward atmospheric moisture transport can be divided into the contributions of mean meridional circulation (MMC), stationary eddies (SE) and transient eddies (TE), i.e. moving cyclones (Palmen and Vuorela, 1963). The total moisture transport to the Arctic is dominated by TE (Peixoto and Oort, 1992; Oshima and Yamazaki, 2004; Sorteberg and Walsh, 2008), but the role of SE has received much less attention.

During recent decades, we have witnessed a strong improvement in the accuracy of atmospheric model analyses, reanalyses and forecasts (Simmons and Hollingsworth, 2002; Uppala *et al*., 2005). Due to changes in models and data assimilation systems, operational analyses do not provide a consistent long-term dataset on the atmospheric moisture budget, but reanalyses based on the utilization of the same model and data assimilation procedure are better in this respect. The potential of reanalyses in investigations of the Arctic moisture budget had been realized by Walsh *et al*. (1994) already before the first reanalyses became available. Several reanalyses are presently available, and in Section 2.1 we select the most suitable one for the present study.

Our study is motivated by the dramatic changes that have been recently observed in the Arctic freshwater system (White *et al*., 2007), which call for more detailed investigations on the atmospheric moisture budget. Our specific objectives are as follows:

1. to provide a comprehensive picture of the horizontal and vertical distribution as well as the meridional transport of water vapour over the circumpolar Arctic in different seasons and to compare it with previous estimates;
2. to analyse the spatial and seasonal distributions of precipitation and evaporation and to compare them with previous estimates;
3. to quantify the role of the MMC, SE and TE in the moisture transport in various regions and seasons;
4. to obtain quantitative results for the net precipitation in the Arctic and to compare them with the water vapour flux convergence, taking into consideration the sources of uncertainty in both results; and
5. to analyse the relationship between the atmospheric moisture budget and large-scale atmospheric circulation, as characterized by the indices of the Arctic Oscillation (AO) and North Atlantic Oscillation (NAO).

The reanalyses and our methodology are described in Section 2, whereas the precipitation and evaporation as well as the vertical and horizontal distribution of water vapour are presented in Section 3. In Section 4, we address the transport of water vapour, and Section 5 focuses to the links between the large-scale circulation indices and variables related to the moisture budget.

2. Data and methodology

2.1. Selection between reanalyses

Some studies on the atmospheric moisture budget in the Arctic (Cullather *et al*., 2000; Boer *et al*., 2001; Rogers *et al*., 2001; Sorteberg and Walsh, 2008) have been based on the reanalysis of the US National Center for Environmental Prediction (NCEP) and National Center for Atmospheric Research (NCAR) or the ERA-15 reanalysis of the European Centre for Medium-Range Weather Forecasts (ECMWF), while the ERA-40 reanalysis (Uppala *et al*., 2005) has been applied by Serreze *et al*. (2006, 2007), Rinke *et al*. (2008). Boer *et al*. (2001) and Rinke *et al*. (2008) also utilized climate model results.

In selecting the data basis for the present study, we paid attention to the accuracy of various reanalyses in the Arctic. Studies on validation and inter-comparison of reanalyses have revealed that NCEP/NCAR reanalysis suffers from serious inaccuracies and general overestimation of the Arctic precipitation. Both precipitation and evaporation are much too high in summer both over land (Serreze and Barry, 2005; Bromwich and Wang, 2008) and the Arctic Ocean (Cheng *et al*., 2008). According to Cullather *et al*. (2000) and Serreze and Barry (2005), in ERA-15 and the original NCEP/NCAR reanalysis (hereafter called as NCEP1) as well as the NCEP-DOE reanalysis 2, the forecast values of annual net precipitation are about 60% lower than the water vapour flux convergence, indicating a severe hydrological imbalance in the model. In the ERA-40 reanalysis, estimates of water

vapour flux convergence are much more closely in balance with the net precipitation (Serreze *et al*., 2006). Furthermore, within the catchment areas or major Arctic rivers, ERA-40 captures much higher percentage of the observed temporal precipitation variance than NCEP1 (Bromwich *et al*., 2007). Although more accurate than NCEP/NCAR, ERA-40 also has certain shortcomings in precipitation estimates over the Arctic. The reanalysis gives generally less precipitation than observations (Serreze *et al*., 2005). On the basis of comparisons of different reanalyses, Serreze *et al*. (2006) estimate that errors in the annual mean water vapour flux convergence over the polar cap (70–90°N) are of 10%. Also, the annual mean runoff and the water vapour flux convergence over the Arctic land areas agree within 10%. The individual terms (precipitation and evaporation) are less certain.

Also with respect to other variables, the quality of the ERA-40 in the Arctic is better than that of the NCEP1 and the Japanese JRA-25 reanalyses (Bromwich *et al*., 2007). Bromwich and Wang (2005) validated ERA-40 against two independent rawinsonde sounding datasets from the Arctic marginal sea ice zone in the late 1980s and early 1990s. The ERA-40 results for the geopotential height, temperature and humidity fields were in close agreement with the observations. The cloud cover and its variability are better captured by ERA-40 than by NCEP1 and JRA-25 (Bromwich *et al*., 2007). Considering moderate to high-intensity cyclones, the climatology based on ERA-40 well corresponds to that based on NCEP1, but there are differences in the climatology of weak cyclones (Bromwich *et al*., 2007). The latter is mostly related to problems in data assimilation (Condron *et al*., 2006). One reason for the success of ERA-40 is that satellite data are used by assimilating raw radiances, which require more computational time but are more accurate than assimilation of vertical temperature and humidity profiles retrieved from the satellite data. Furthermore, ERA-40 is based on a model with a higher vertical resolution (60 layers) than those used for NCEP/NCAR (28 layers) and JRA-25 reanalyses (40 layers).

An initial validation of the ERA-Interim reanalyses has shown very promising results (Simmons *et al*., 2007). Unfortunately, only 10 years of ERA-Interim data were available when we started the present study. On the basis of the above, we selected ERA-40 reanalysis as the basis of the present study. The ERA-40 reanalysis has already been utilized in comprehensive studies of the Arctic large-scale energy budget (Serreze *et al*., 2007) and freshwater cycle (Serreze *et al*., 2006), but our objectives (listed in Section 1) include many aspects that have not received detailed attention in the previous studies.

2.2. ERA-40 reanalysis

The ERA-40 reanalysis covers 44 full years from 1958 to 2001 and is based on a forecast model at T159 resolution (approximately 125 km in the horizontal). The temporal resolution is 6 h and the vertical resolution is 60 levels, of which more than half are in the troposphere. In this study, we apply data from the lowest 27 levels of ERA-40. The uppermost one is approximately at 300 hPa pressure level. The error caused by the reduced number of levels is about 1% for the vertically integrated water vapour.

Specific humidity, northward wind, surface pressure, 2-m air temperature, precipitation, evaporation and vertically integrated water vapour flux convergence were collected from the ECMWF data archive in a $1^\circ \times 1^\circ$ grid covering the region 55–90°N. The area averages were calculated separately for the polar cap, 70–90°N, which allowed us to directly compare results with many previous studies.

Precipitation and evaporation are from forecast fields, whereas the other variables are analyses based on 6-h forecasts (as the first-guess field) and assimilated observations. A three-dimensional variational data assimilation (3DVAR) technique is used (Uppala *et al*., 2005). The water vapour data assimilated into ERA-40 are humidity profiles from radiosondes and, since 1979, raw radiances from a number of satellite instruments.

Over snow- and ice-covered regions, remote sensing data on air humidity were, however, not assimilated to ERA-40. This is due to the difficulties in distinguishing between the signals originating from the surface and the atmosphere. The sea ice concentration, which is important for evaporation (Valkonen *et al*., 2008), is based on satellite measurements from the Special Sensor Microwave Imager (SSM/I) using two-dimensional variational data assimilation (Fiorino, 2004). Over the Arctic, the effects of data assimilation on the ERA-40 wind field arise from the surface pressure observations from drifting buoys and terrestrial stations, as well as from the satellite-based temperature profile data.

To avoid errors due to the model spin-up period (Bromwich *et al*., 2002; Tietäväinen and Vihma, 2008), we have made use of 24-h forecasts. Serreze *et al*. (2006) based their study on 6-h forecasts, but recognized that the spin-up problem tends to generate a small negative bias.

2.3. Moisture calculations

To calculate the total water vapour content, integrations through an atmospheric column were made from the surface pressure p_1 to the 27th level pressure p_{27}. Taking a vertical integral of specific humidity q (g kg^{-1}) through an atmospheric column, we get integrated precipitable water vapour (IPWV) (kg m^{-2} or mm):

$$IPWV = -\frac{1}{g} \int_{p_1}^{p_{27}} q \quad dp, \tag{1}$$

where g is the acceleration due to gravity.

For the vertically integrated meridional moisture flux (MMF) (kg m^{-1} s^{-1}), we get:

$$MMF = -\frac{1}{g} \int_{p_1}^{p_{27}} q \cdot v \quad dp, \tag{2}$$

where v is the northward wind component. MMF can be divided in the contributions of MMC, SE and TE (Palmen and Vuorela, 1963):

$$\underbrace{[\overline{qv}]}_{\text{MMF}} = \underbrace{[\overline{q}]\,[\overline{v}]}_{\text{MMC}} + \underbrace{[\overline{q}^*\overline{v}^*]}_{\text{SE}} + \underbrace{[\overline{q'v'}]}_{\text{TE}}, \tag{3}$$

where the overbar denotes temporal averaging and square brackets denote zonal averaging, and the prime and the star denote deviations from the temporal and zonal means, respectively. The deviations from the temporal mean were calculated from the temporal mean for each month. Hence, the TE term does not include the contribution of seasonal and inter-annual variations, but is related to synoptic-scale transient cyclones. The components of vertically integrated water vapour flux are:

$$\begin{aligned} MMF = & \underbrace{-\frac{1}{g}\int_{p_1}^{p_{27}} [\overline{q}]\cdot[\overline{v}]\quad dp}_{\text{MMC}} \\ & \underbrace{-\frac{1}{g}\int_{p_1}^{p_{27}} [\overline{q}^*\overline{v}^*]\quad dp}_{\text{SE}} \\ & \underbrace{-\frac{1}{g}\int_{p_1}^{p_{27}} [\overline{q'v'}]\quad dp}_{\text{TE}}. \end{aligned} \tag{4}$$

For analyses of the dependence of the moisture budget on large-scale circulation conditions, we used station-based seasonal average indices of NAO obtained from the NCAR Climate Global Dynamics Division (http://www.cgd.ucar.edu/cas/jhurrell/indices.data.html#naostatseas) and monthly mean indices of AO based on empirical orthogonal function (EOF) method, obtained from the NOAA Climate Prediction Center (http://www.cpc.ncep.noaa.gov/products/precip/CWlink); the seasonal values were calculated as averages of the monthly means.

2.4. Selection of the study period

The time series of the annual means of IPWV, 2-m air temperature, precipitation, evaporation and net precipitation over the polar cap (70–90°N) are presented in Figure 1. We divided the time series in two periods: before the era of satellite data assimilation (1958–1978) and during the satellite era (1979–2001), and used the F-test to study the statistical significance of the linear trends. Coefficients of determination (r^2) between the year and the variables (annual means over the polar cap) are presented in Figure 1, and trends of the time series are presented in Table I.

For the whole period (1958–2001), the trends of all variables, except IPWV, are statistically significantly (95%) positive (Table I). Before the satellite era, the trends in the IPWV, precipitation and net precipitation are statistically significantly positive, whereas there is no significant trend in air temperature and evaporation. During the satellite era, the only significant trend is found in the 2-m air temperature. Previous studies based on ERA-40 but for partly different regions have indicated that there is no significant trend in IPWV for 1958–2001 at 60–90°N (Rinke *et al*., 2008), and no significant trend in the net precipitation over the Arctic Ocean during 1979–2001 (Serreze *et al*., 2006).

Trend assessments from reanalysis are fraught with uncertainty (Trenberth *et al*., 2005; Trenberth and Smith, 2006; Serreze *et al*., 2007), and instead of quantifying trends our purpose is to eliminate periods for which ERA-40 is not reliable enough. Trends in the study quantities show remarkable changes around 1979. We cannot be sure how large portions of these changes can be explained by the assimilation of satellite data and by decadal changes in the large-scale atmospheric circulation (Section 5), and we therefore adopt a careful approach and include in the analyses data from 1979 to 2001 only.

3. Air moisture in the Arctic

This study concentrates on the water vapour; cloud liquid water and ice water are not included. In polar regions, as an annual mean, water vapour represents approximately 99% of the total water content (vapour, liquid and ice) in the atmosphere (Tietäväinen and Vihma, 2008).

3.1. Specific humidity and IPWV

Vertical cross-sections of specific humidity q along longitudes 0, 90, 180 and 270°E are shown in Figure 2. Due to decreasing temperature, the isolines of q are slanting towards north. Zonal variations in the profiles of q are mainly constrained to altitudes lower than the 500 hPa pressure level. At higher altitudes, q is mostly controlled by the latitude and season.

Below the 850-hPa level, there are inversions in specific humidity during all seasons, but particularly in winter. At longitudes 90, 180 and 270°E, winter inversions occur from 65°N to the Pole, and at 0°E from 82°N to the Pole (all details cannot be detected from Figure 2). In winter, the inversions are deep (1200 m), strong (up to 0.3 g kg^{-1}) and sharp, typically from -0.002 to -0.005 g kg^{-1} hPa^{-1}. In spring and autumn, the inversions are usually elevated with the base between 990 and 900 hPa levels, and the inversion depth usually less than 400 m, strength 0.1 g kg^{-1} and the magnitude of the gradient less than 0.002 g kg^{-1} hPa^{-1}. In summer, there are small regions with strong but shallow ground-based inversions, with the magnitude of the gradient even more than 0.005 g kg^{-1} hPa^{-1}. A potential mechanism for their generation is that warm, humid air is advected from over the continents, and the atmospheric boundary layer is cooled over the Arctic Ocean, so that the specific humidity is restricted by the low saturation humidity of the cold air.

Mean values of IPWV for the polar cap (70–90°N) are 4.0 mm in spring, 12.3 mm in summer, 5.5 mm in autumn and 2.4 mm in winter (Table II). The seasonal fields of IPWV for years 1979–2001 are presented in

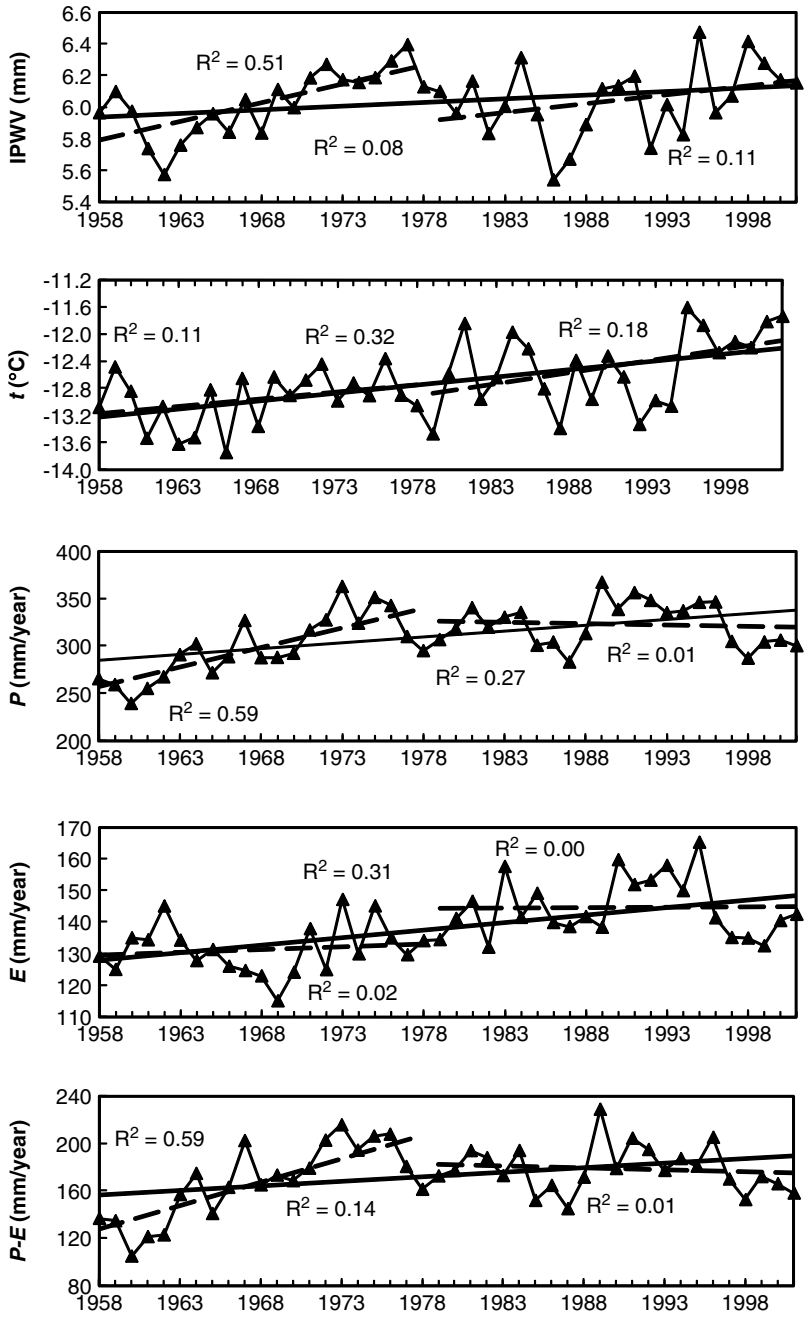

Figure 1. Time series of the annual means of the IPWV (mm), 2-m air temperature (°C), precipitation (mm year^{-1}), evaporation (mm year^{-1}), and net precipitation (mm year^{-1}) for the region from 70 to 90°N. The coefficient of determination (R^2) is marked for periods 1958–1978, 1958–2001 and 1979–2001.

Table I. Trends of time series of annual mean IPWV, 2-m air temperature, precipitation, evaporation and net precipitation over the region from 70 to 90°N.

Variable	Unit	1958–1978	1979–2001	1958–2001
IPWV	mm	**0.024**	0.011	0.005
Air temperature	^{o} C	0.021	**0.035**	**0.024**
Precipitation	mm year^{-1}	**4.090**	−0.311	**1.238**
Evaporation	mm year^{-1}	0.175	0.035	**0.476**
Net precipitation	mm year^{-1}	**3.915**	−0.346	**0.761**

Statistically significant (95%) trends are marked in bold.

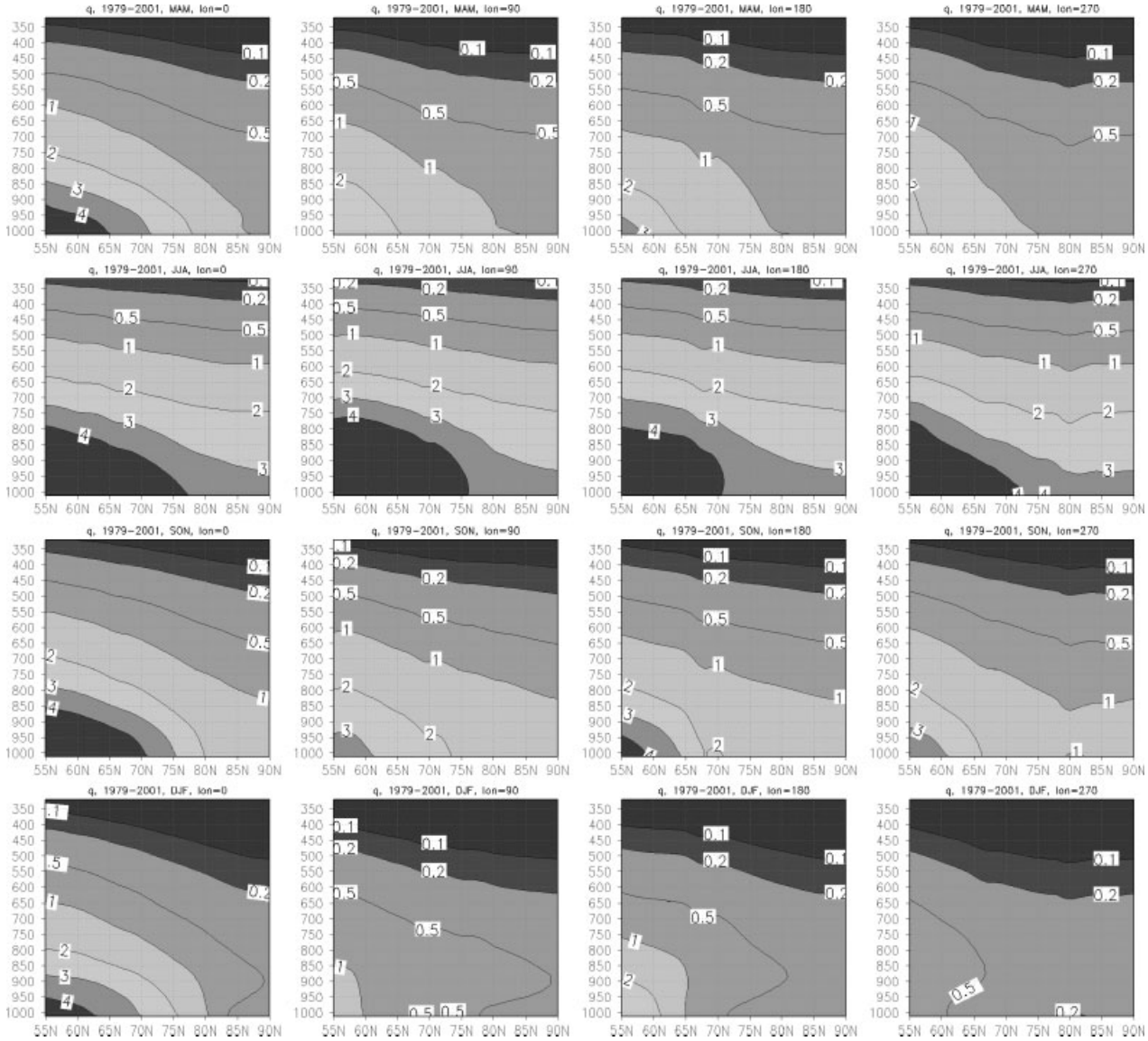

Figure 2. Seasonal mean cross-sections of the specific humidity q (g kg^{-1}) at the longitudes 0°, 90°, 180° and 270 °E for years 1979–2001.

Table II. Seasonal averages over the polar cap (70–90 °N) for years 1979–2001. Moisture transport is defined positive northwards.

Quantity	Unit	MAM		JJA		SON		DJF		Year	
		Aver.	STD	Aver.	STD	Aver.	STD	Aver.	STD	Aver.	STD
Meridional moisture flux	kg m^{-1} s^{-1}	3.49	0.72	7.04	0.94	4.98	0.66	3.19	0.59	4.67	0.44
Mean meridional circulation	kg m^{-1} s^{-1}	0.38	0.32	0.64	0.53	0.39	0.42	0.41	0.24	0.46	0.28
Stationary eddy	kg m^{-1} s^{-1}	0.05	0.36	0.18	0.66	0.35	0.44	0.03	0.53	0.15	0.20
Transient eddy	kg m^{-1} s^{-1}	3.06	0.42	6.22	0.59	4.25	0.49	2.74	0.42	4.07	0.33
Precipitable water	mm	4.0	0.2	12.3	0.6	5.5	0.3	2.4	0.2	6.1	0.2
Temperature	°C	−15.2	0.9	1.7	0.3	−11.6	0.9	−24.8	1.1	−12.5	0.6
Evaporation	mm	32.4	3.3	40.5	2.1	40.6	4.9	31.3	3.2	144.7	9.4
Precipitation	mm	60.1	7.7	103.5	12.1	95.2	5.9	64.5	6.9	323.4	22.8
Net precipitation	mm	27.7	6.1	63.1	12.0	54.6	6.9	33.3	7.0	178.7	19.5
Convergence	mm	38.2	6.6	70.1	7.6	50.3	8.0	33.9	7.0	192.4	15.5
$P - E -$ conv.	mm	−10.5	2.9	−7.1	7.0	4.4	0.6	−0.6	3.1	−13.8	10.6

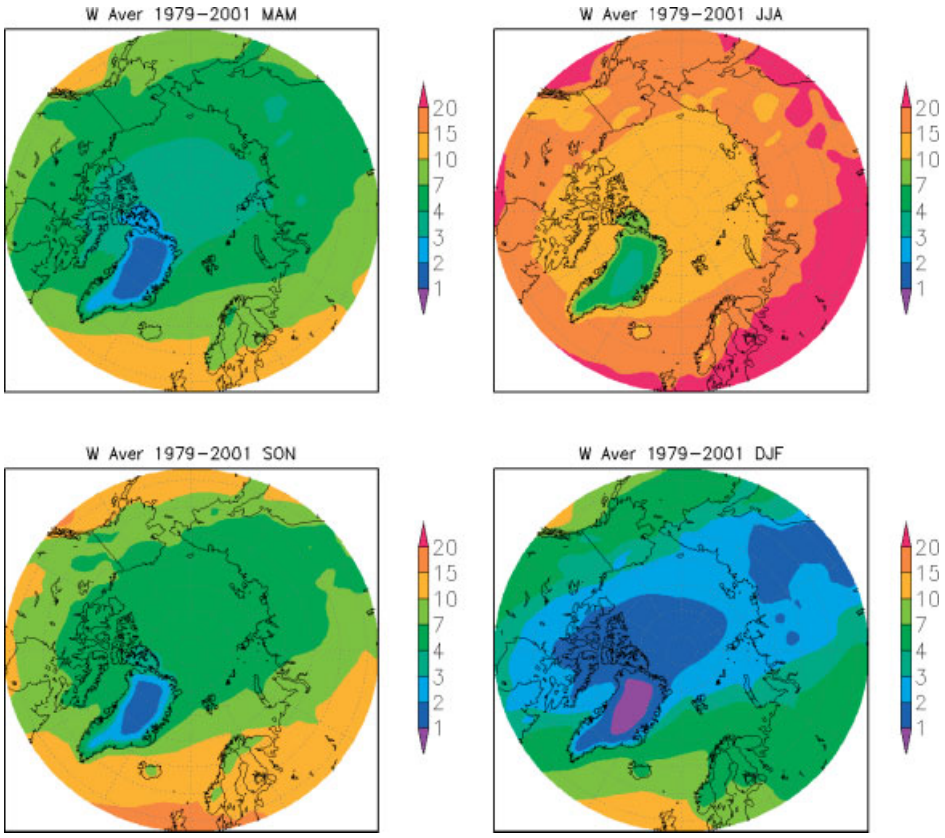

Figure 3. Seasonal mean IPWV (mm) for years 1979–2001. This figure is available in colour online at wileyonlinelibrary.com/journal/joc

Figure 3. Higher values occur at the Atlantic sector; only in summer the highest values along a zonal belt occur over continental Europe and western Asia. Smallest values occur over the high ice sheet of Greenland, where the average value of IPWV is below 4 mm even in summer.

Seasonal variability in IPWV strongly depends on the location. Higher variability (summer mean more than five times the winter mean) takes place in a region covering Canada except Rocky Mountains, the Arctic Ocean and Siberia. The variability is highest – more than 11 times – in the region south of Yakutsk, where in summer the average value exceeds 20 mm, whereas in winter the average value is 1–2 mm. Smaller (less than five times) variability occurs over the Atlantic Ocean, Europe, southern Greenland, the Bering Sea, Alaska and Rocky Mountains in Canada. The variability is smallest – less than two times – in Scotland region, where all seasonal averages are in the range of 10–20 mm. The IPWV mean values are fairly similar in the transition seasons: in the whole study area, the autumn values are 1.3 ± 0.2 times higher than spring ones. This shows that local factors, such as latitude, altitude and surface type, do not play a large role for the autumn/spring ratio in IPWV (in contrast to the summer/winter ratio).

Over the oceans, the variability in IPWV relates very strongly to changes in sea surface temperature and is coherent with the assumption of a fairly constant relative humidity (Trenberth *et al*., 2005). The isolines of IPWV are prolonged in the eastern Canada–Siberia axis during all seasons, with the maximum asymmetry in winter, when the heat and moisture sources in the Atlantic and Pacific sectors keep the IPWV large. In summer, the asymmetry decreases as a result of enhanced evaporation over warm land surfaces (Walsh *et al*., 1994).

The distributions of specific humidity and IPWV based on ERA-40 agree well with the rawinsonde-based results for the zonal means at 70°N (Serreze *et al*., 1995b), but distributions based on other reanalyses do not seem to have been published. Validating the results of the regional climate model HIRHAM, Rinke *et al*. (2008) found that for 1958–2001 in the region north of 60°N the IPWV values based on HIRHAM were lower than those of ERA-40 with a maximum difference of 1 mm in July.

3.2. Precipitation and evaporation

Seasonal fields of precipitation P for years 1979–2001 are presented in Figure 4. In the polar cap area (70–90°N), there is more precipitation in summer (104 mm) and autumn (95 mm) than in winter (65 mm) and spring (60 mm) (Table II). The summer peak in P is largely associated with convective precipitation. Smallest values – less than 30 mm per season – occur in northern Greenland. Small values also occur from Canada to Asia in winter and spring. Highest values of precipitation – more than 500 mm per season – occur at coastal areas of North Pacific Ocean in autumn and winter

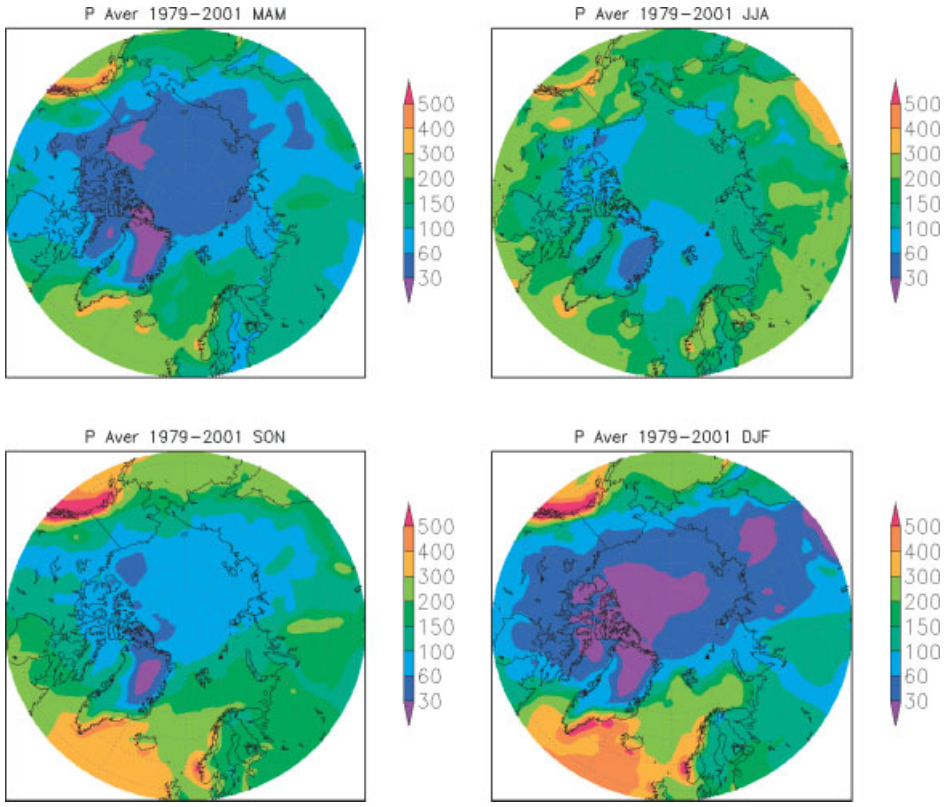

Figure 4. Seasonal mean precipitation P (millimetres per season) for years 1979–2001. This figure is available in colour online at wileyonlinelibrary.com/journal/joc

and, in winter, at the southeastern coast of Greenland and southwestern coast of Norway. It is noteworthy that in the North Atlantic region the annual maximum precipitation occurs in winter, although over the whole study region as a mean, winter is the second driest season after spring. Winter maximum is related to the seasonality in the strength of the North Atlantic cyclone track. Net precipitation is discussed in Section 4.3.

Utilizing several station datasets (with corrections for gauge undercatch) and forecasts from the NCEP1 reanalysis (with corrections for systematic biases), Serreze and Barry (2005) analysed the spatial distributions of precipitation in the Arctic. They presented results for January, April, July and October. Multiplying their monthly values by 3, their results compare well with the magnitudes of ERA-40 seasonal precipitation. In ERA-40, however, the regions of minimum values are shifted more to the Arctic Ocean, while in Serreze and Barry (2005) the minima are more centred over the Canadian archipelago. Serreze *et al*. (2005, 2006) compared ERA-40 precipitation with observations: both over the ocean and land the ERA-40 results are approximately 10% lower than observations, but the differences are within the error margins of the observations.

Bromwich *et al*. (2002) reported a systematic cold bias over the Arctic in an initial ERA-40 dataset for years 1989–1992. The bias was due to assimilation of the high-resolution infrared radiometer (HIRS) data. The bias was largest over sea ice and more pronounced in summer, and may have contributed to the anomalously high summer precipitation in the central Arctic (Serreze and Etringer, 2003). In the final ERA-40 dataset, the HIRS data assimilation procedure is corrected for years 1979–1988 and 1997–2002, which removed the Arctic Ocean cold bias from these years (Uppala *et al*., 2005; Bromwich *et al*., 2007). The bias is, however, still present in ERA-40 in the period of 1989–1996 (Uppala *et al*., 2005).

Seasonal fields of evaporation E (millimetre per season; for evaporation over the sea and evapotranspiration over land, we simply use the term evaporation) for years 1979–2001 are presented in Figure 5. In the area north of 70°N (Table II), the evaporation is stronger in autumn (41 mm) and summer (40 mm), and weaker in spring (32 mm) and winter (31 mm). Smallest values – less than 10 mm per season – occur in all seasons except summer in Greenland and the Arctic Ocean. Highest values of evaporation – more than 300 mm per season – occur over the North Atlantic Ocean in winter.

Serreze *et al*. (2006) found that the ERA-40 evaporation over the Arctic land areas is 20–50% larger than observed, and according to Betts *et al*. (2003) the overestimation is 30% in the Mackenzie River basin. Serreze *et al*. (2006) further concluded that the best estimate for evaporation is based on a residual of observed precipitation and ERA-40-based water vapour flux convergence. Also, previous reanalyses have suffered from too large evaporation: Cullather *et al*. (2000) concluded that north of 70°N both ERA-15 and NCEP/NCAR reanalyses had at least 40% too large evaporation.

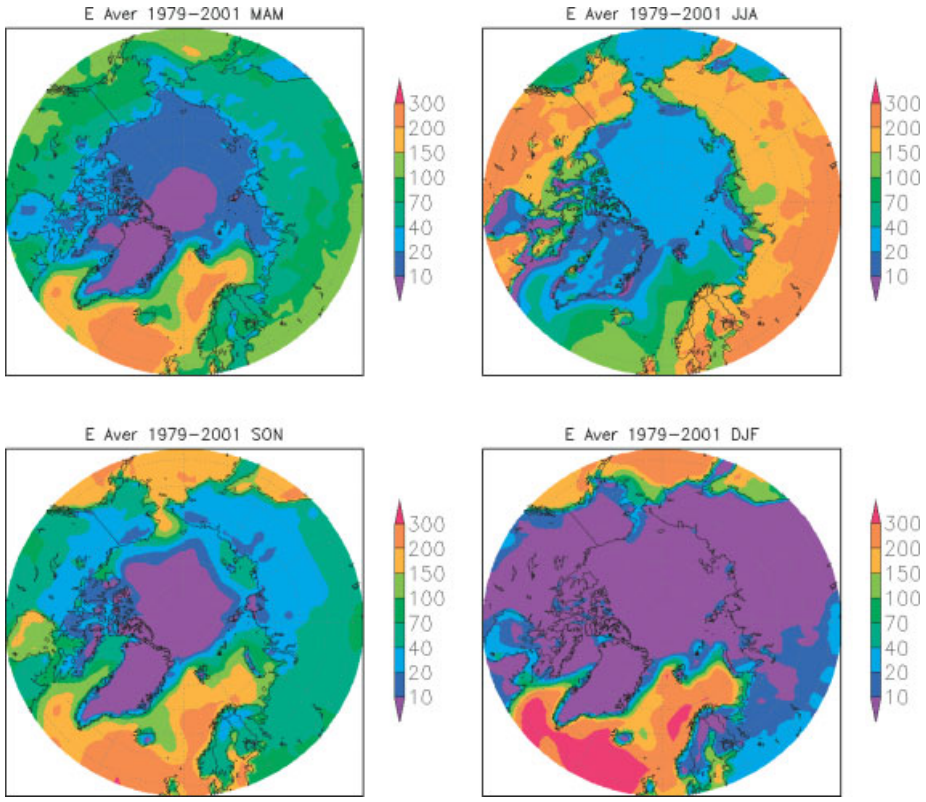

Figure 5. Seasonal mean evaporation E (millimetres season) for years 1979–2001. This figure is available in colour online at wileyonlinelibrary.com/journal/joc

Walsh *et al*. (1994) calculated evaporation as a residual term of moisture flux convergence (based on rawinsonde data) and precipitation observations and got values slightly smaller than those based on ERA-40: 133 and 145 mm, respectively. Their seasonal averages for the polar cap were in autumn and winter 5 mm and in spring 12 mm smaller than ERA-40 data, whereas their summer average exceeded the ERA-40 value by 11 mm. The origin of the difference in summer evaporation probably lies in too small a flux convergence in the Walsh *et al*. (1994) dataset in summer (26% smaller than in ERA-40), whereas in other seasons the difference is less than 6%. The differences in precipitation were less than 13% in all seasons.

4. Moisture transport to the Arctic

The moisture transport to the Arctic is governed by large-scale circulation patterns. The mid-tropospheric large-scale circulation in the Arctic is characterized by the polar vortex, which in winter is strong and asymmetric, with major troughs in eastern North America and eastern Asia (Serreze and Barry, 2005). The polar vortex becomes weaker and more symmetric during spring and summer. At the sea level, the mean winter circulation is dominated by the Icelandic Low, the Aleutian Low and the Siberian High, whereas in summer the large-scale circulation is much weaker. The MMC north of approximately 50°N is related to the Polar cell characterized by ascending motion in the sub-polar latitudes (50°–70°), descending motion over the Pole, pole-ward motion aloft and equator-ward motion near the surface. The Polar cell is, however, asymmetric, much weaker and much more disturbed by TE than the Hadley and Ferrell cells. The mean zonal and meridional circulations are also strongly affected by the AO (Boer *et al*., 2001).

4.1. Distribution of total meridional moisture transport

Seasonal distribution of vertically integrated meridional water vapour flux MMF is presented in Figure 6. Seasonal mean values for the polar cap range from 3.2 kg m^{-1} s^{-1} in winter to 7.0 kg m^{-1} s^{-1} in summer (Table II). The MMF values are highest in summer because of the abundance of moisture (Sorteberg and Walsh, 2008). Major northward MMF takes place in the Atlantic sector and North Pacific Ocean. The peak northward transport in the Atlantic sector is primarily due to a high mean specific humidity and the frequent advection of moisture by TE (Serreze *et al*., 1995a, 1995b). Major southward MMF takes place in the Canadian sector, especially in summer, but totally it is much weaker than the northward transport. In all seasons, there is a notable clockwise transport of moisture around Greenland.

Seasonal contribution to annual mean moisture transport into the polar cap is higher in summer (36%) and lower in autumn (26%), spring (20%) and winter (18%). These results coincide very well, within 2% at every season, with Dickson *et al*. (2000), based on rawinsonde dataset, and Sorteberg and Walsh (2008), based

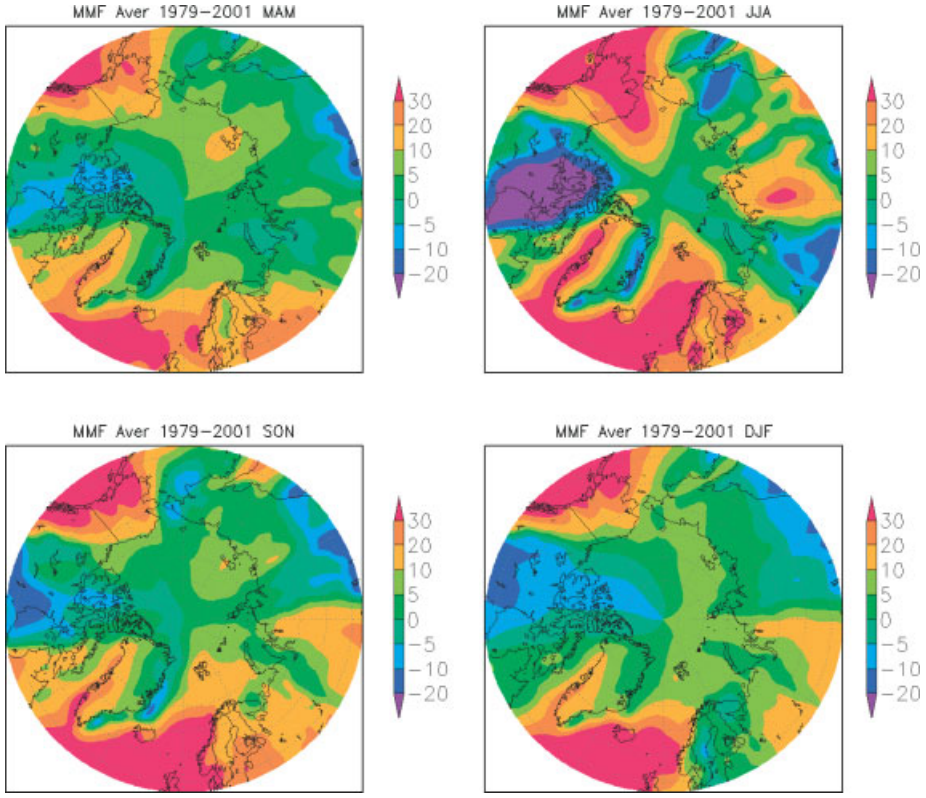

Figure 6. Seasonal mean meridional moisture flux MMF (kg m^{-1} s^{-1}, positive northwards) for years 1979–2001. This figure is available in colour online at wileyonlinelibrary.com/journal/joc

on NCEP1 reanalysis. Satellite-based seasonal transports for 1980–1993 found by Groves and Francis (2002) had, however, a considerably higher contribution in spring (25%), whereas in other seasons the contributions were some percent less than our values.

MMF vertical profiles calculated for 1-hPa layer thickness are presented in Figure 7. In the Atlantic cross-section (0 °E), there is a deep layer of a strong northward moisture transport. Close to the surface, a weak southward transport takes place. The second strongest northward transport takes place in the Russian cross-section (90 °E), but compared with the Atlantic cross-section the transport is located at lower altitudes. In summer, there is a sharp difference in the moisture transport between continents and the sea, with a strong northward transport over the land but even weak southward transport over the sea. At the Bering Sea cross-section (180 °E), southward moisture transport takes place during spring and autumn at pressure levels below 700 hPa at the East Siberian latitudes, whereas northward transport prevails almost everywhere else. At the Canadian cross-section (270 °E), southward transport usually dominates. The strongest northward transport north of 80°N locates, however, in this cross-section in summer. Figure 7 also demonstrates that in summer and autumn the largest moisture transport (>2.5 kg m^{-1} s^{-1} hPa^{-1}) takes place in a much thicker air column than in winter.

The zonal differences are related to differences in the cyclone activity. The Polar cell would favour southward moisture transport in the lower troposphere, but at most longitudes and seasons the cyclone-related contributions dominate generating a northward transport (Section 4.2). According to Serreze *et al*. (1995b), on the basis of rawinsonde data the zonal mean v at 70°N is southward up to 400 hPa, but in ERA-40 it is southward only up to 950 hPa and northward above. In the Canadian Arctic archipelago, however, the mean southward wind is strong (1.4 m s^{-1}) at least up to the 300-hPa level and cyclone activity weak, making it the primary region of southward moisture transport.

On the basis of rawinsonde data, Overland and Turet (1994) and Serreze *et al*. (1995a, 1995b) found out that the pole-ward moisture transport at 70°N tends to peak in the lower troposphere, typically at about the 850-hPa level. This represents the 'trade-off' level between the effects of specific humidity decreasing with height and winds increasing with height. We found that in ERA-40 the peak transport usually occurs below the 900-hPa pressure level: this is the case for 94% of the data in autumn, 87% in spring, 77% in summer and 63% in winter. The median peak occurs in winter at 930 hPa pressure level and in other seasons at 970–990 hPa level, which clearly differ from the 850 hPa based on coarse-resolution rawinsonde data (Overland and Turet, 1994; Serreze *et al*., 1995a, 1995b).

4.2. Division of the moisture transport to TE, SE and MMC

The seasonal means of the contributions of TE and SE transports to the meridional moisture flux MMF are

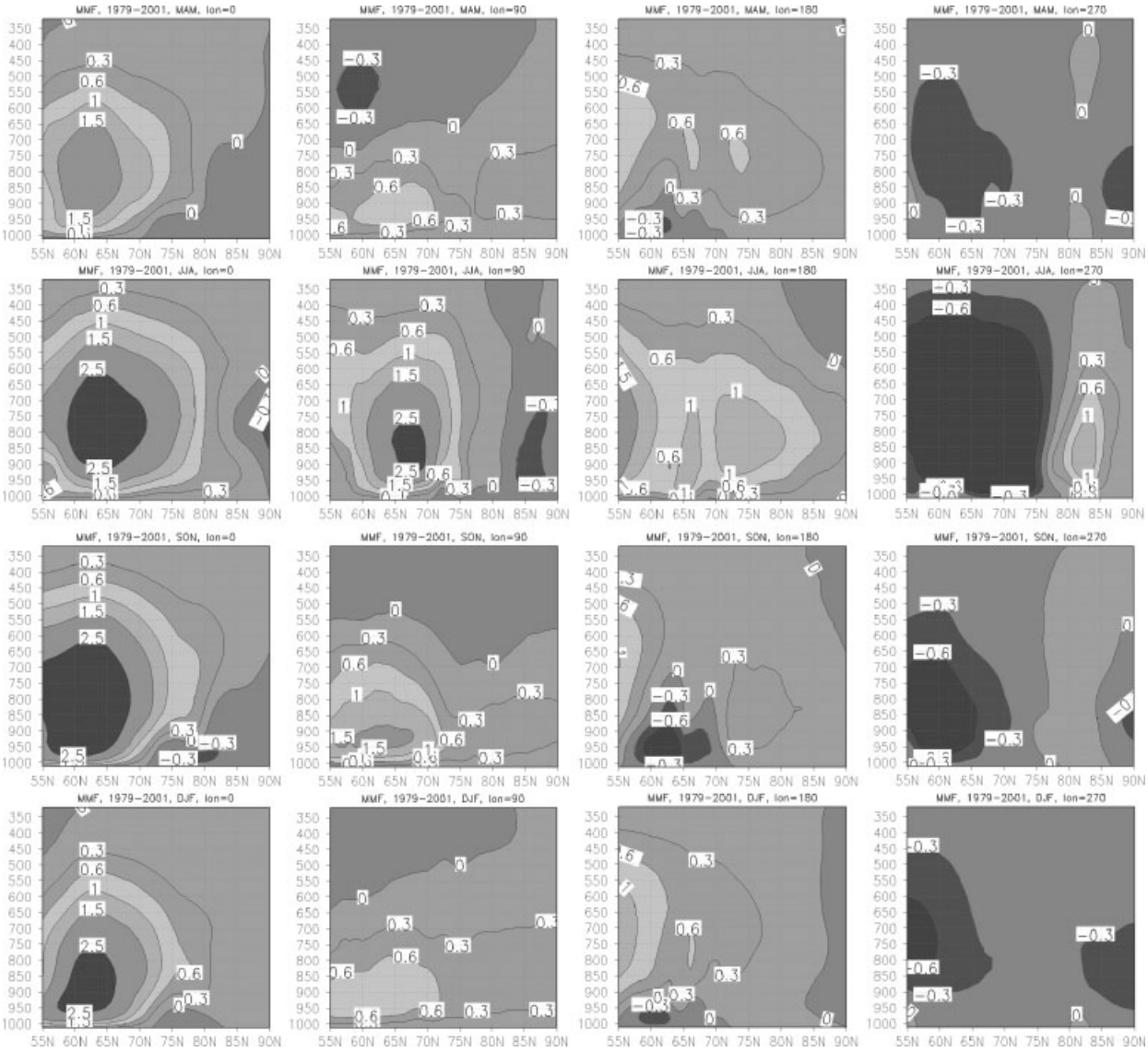

Figure 7. Meridional moisture flux MMF (kg m^{-1} s^{-1} hPa^{-1}) seasonal average cross-sections at the longitudes of 0, 90, 180, and 270 °E for years 1979–2001.

shown in Figure 8. Statistically, TE is the covariance between specific humidity q and meridional wind component v. TE is northward almost everywhere: i.e. positive anomalies of specific humidity and northward wind usually occur simultaneously. Oshima and Yamazaki (2006) showed that in summer TE is controlled mostly by the moisture effect, whereas in winter by the eddy effect. This is in agreement with the fact that cyclones are generally more intense in winter than in summer (Zhang *et al*., 2004).

Higher values of TE are located in the Atlantic and Pacific regions. These are due to a larger contrast in specific humidity between cases of northerly and southerly winds. Lower values are located in western Canada and central Asia.

The area average values of SE transport are higher in autumn and smaller in winter and spring (Table II). The SE transport is considerable only at small regions – in the Atlantic sector, Greenland, lower latitudes at central Asia, and the western coast of Canada. Except of the central Asia, these regions are related to the Icelandic and Aleutian lows. The SE transport is negative in western Greenland and positive in summer and autumn in eastern Greenland (Figure 8), but MMF has the opposite pattern (Figure 6). This can be explained by the definition (Equation (3)): SE is product of two components – specific humidity deviation from the zonal average, and northward wind speed deviation from the zonal average. Over Greenland, the specific humidity deviation from the zonal mean is negative, and the meridional wind deviation from the zonal mean is positive in western Greenland but negative in eastern Greenland. Hence, over Greenland the stationary eddy transports moisture in the direction opposite to the actual transport (MMF). Over the western coast of Canada, the situation is analogous to western Greenland: MMF is positive but SE is negative, especially in summer. The tendency of the stationary eddy to transport moisture southward is caused by a humidity lower than

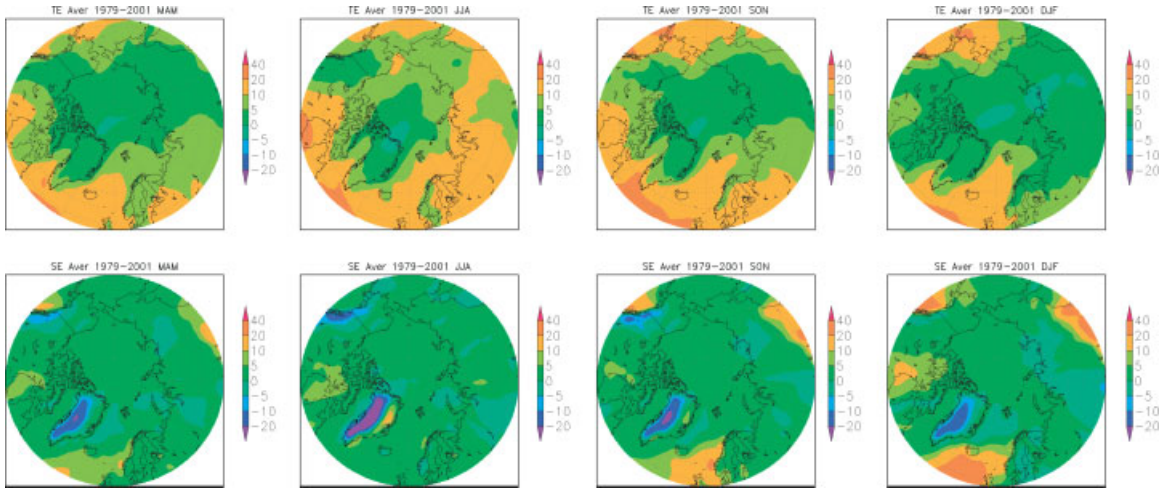

Figure 8. Seasonal mean moisture transport (kg m^{-1} s^{-1}) by standing eddies (SE) and transient eddies (TE) for years 1979–2001. This figure is available in colour online at wileyonlinelibrary.com/journal/joc

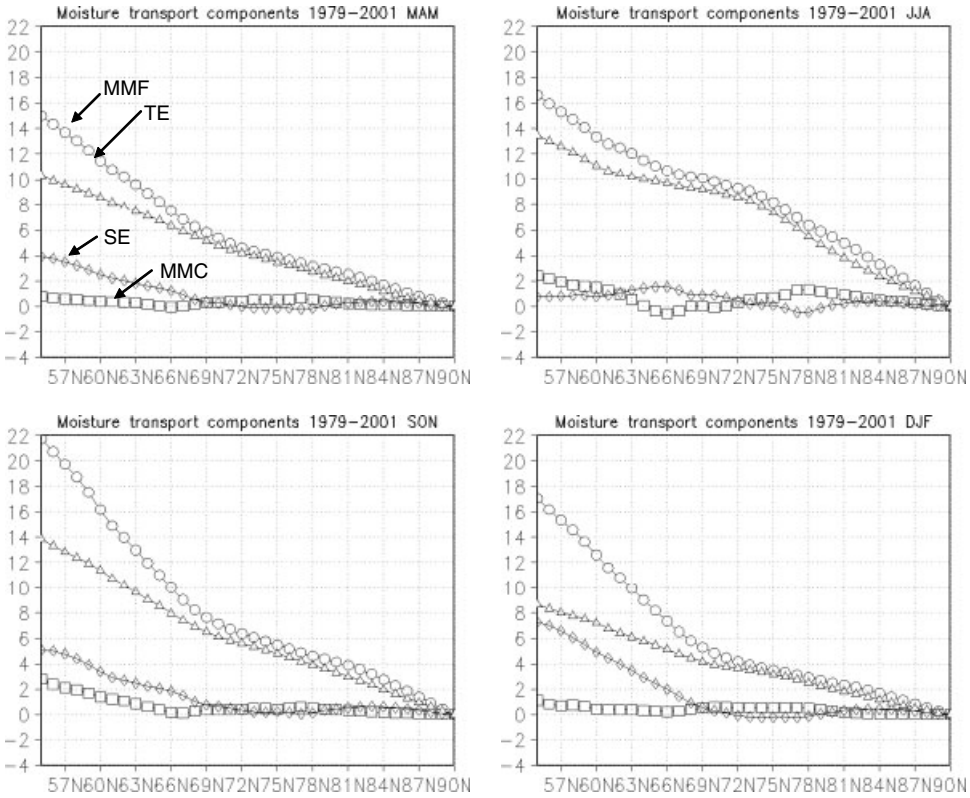

Figure 9. Seasonally and zonally averaged meridional moisture flux (MMF, kg m^{-1} s^{-1}) for years 1979–2001 divided into the contributions of mean meridional circulation (MMC), stationary eddies (SE) and transient eddies (TE).

the zonal mean combined with northward wind higher than the zonal mean: i.e. there is actually northward transport of drier air. In the central Asia, the SE component is positive, but is actually caused by lower than average humidity with lower than average northward wind.

The zonal mean transports are shown in Figure 9. As is well known (Overland and Turet, 1994; Sorteberg and Walsh, 2008), the TE are responsible for most of the northward water vapour transport in high latitudes. In ERA-40, their contribution of MMF across 70°N ranges from 81% in winter to 92% in summer (qualitatively seen from Figure 9). North of the Arctic Circle, the effect of SE is small (<1 kg m^{-1} s^{-1}) in every season. In summer, the SE effect is small at all latitudes but at other seasons, especially in winter, it grows southward of 68°N and at 55°N reaches in winter a value of 7.3 kg m^{-1} s^{-1}, comparable to the TE value of 8.7 kg m^{-1} s^{-1}. The contribution by SE to the northward water vapour transport across 70°N ranges from 5 to 9%. The role of MMC in the moisture transport is small: MMC reaches maximally 2.5 kg m^{-1} s^{-1} in summer and autumn at lower latitudes (14% of MMF), whereas in spring and

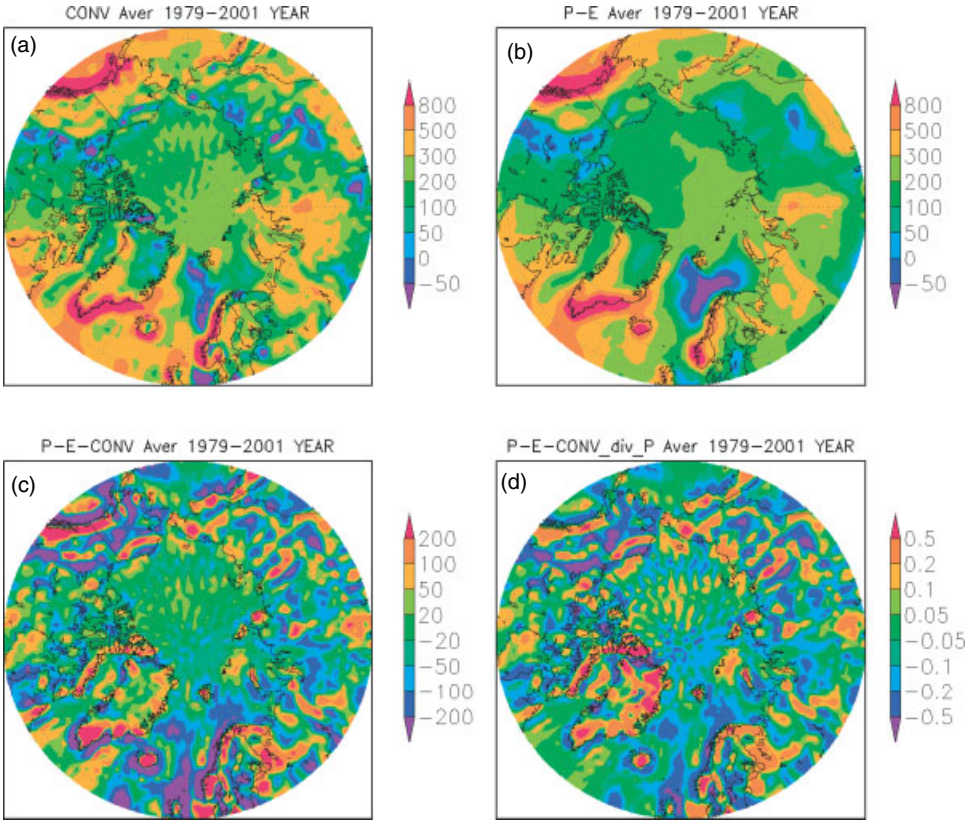

Figure 10. Annual means in 1979–2001 of (a) water vapour flux convergence (mm year^{-1}), (b) net precipitation (mm year^{-1} water equivalent), (c) difference between flux convergence and net precipitation (mm year^{-1}) and (d) difference between flux convergence and net precipitation divided by precipitation. This figure is available in colour online at wileyonlinelibrary.com/journal/joc

winter the contribution is maximally 7% of MMF. North of 70°N, MMC is larger only in summer around 78°N, where it represents 25% of MMF. The contribution of MMC to the northward water vapour transport across 70°N ranges from −1% in summer to 12% in winter.

4.3. Comparison of moisture flux convergence and net precipitation

The ERA-40-based annual mean net precipitation (precipitation plus condensation minus evaporation) for the polar cap north of 70°N is 179 mm and the moisture flux convergence is 192 mm for years 1979–2001 (Table II). As the ERA-40 precipitation is probably too low, whereas the evaporation is too large (Section 3.2), it is not surprising that the ERA-40 net precipitation is lower than the water vapour flux convergence. Flux convergence results based on ERA-15 and NCEP/NCAR range from 182 to 207 mm (Cullather *et al*., 2000). According to Sorteberg and Walsh (2008), estimates of the moisture flux convergence into the polar cap range from 50 mm year^{-1}, based on surface (P and E) observations to 206 mm year^{-1} based on NCEP/NCAR reanalysis for 1980–2001. The ERA-40 flux convergence result is in good agreement with Serreze and Barry (2005), who concluded from NCEP1 reanalysis the value to be 188 ± 6 mm year^{-1}. It is also very close to the 194 mm year^{-1} estimated from NCEP/NCAR reanalysis for 1979–1993 (Cullather *et al*., 2000). Comparing the moisture flux convergence against precipitation, we find, however, a larger discrepancy between ERA-40 and NCEP1. In ERA-40, the moisture flux across 70°N accounts for 59% of the annual Arctic precipitation, whereas in NCEP1 it is 72% (Sorteberg and Walsh, 2008).

The annual mean values of the moisture flux convergence, net precipitation, as well as their absolute and relative differences are shown in Figure 10. The moisture flux convergence reaches its maximum values in the Gulf of Alaska and the surrounding coasts, south and southeast of Greenland, and around the coasts of Iceland, Scotland and Norway. The minimum values are reached in the North Sea, Norwegian Sea, northwestern Greenland Sea and in scattered locations in central and northern Canada and eastern Siberia. The distribution of net precipitation is qualitatively similar. The absolute difference field (Figure 10(c)) includes, however, values with magnitudes exceeding 200 mm year^{-1}. Large differences occur over areas with much topographic variations, which is understandable as the calculation of the flux convergence requires information from neighbouring grid cells, whereas the net precipitation refers to a single grid cell (Calanca and Fortelius, 1996). In addition, large absolute differences occur in regions where the net precipitation is large. The regional differences in Figure 10(c) are much larger than the zonal mean differences in the moisture transport across 70°N reported in Serreze *et al*. (2007). A larger flux convergence is common in sea areas with a

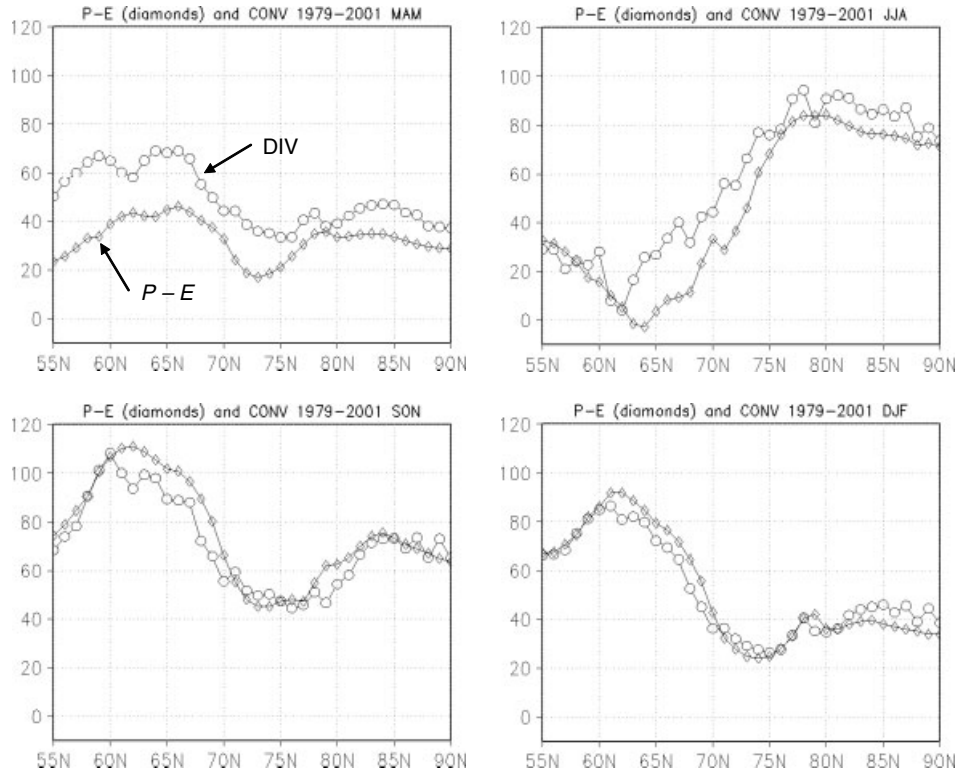

Figure 11. Seasonally and zonally averaged net precipitation (lines with diamonds) and water vapour flux convergence (lines with circles) for years 1979–2001 (in millimetre per season).

high cyclonic activity, such as the Norwegian and Iceland Seas and the Gulf of Alaska, whereas a larger net precipitation is typical for the neighbouring land areas. Over flat surfaces, the relative differences are almost independent of the latitude (Figure 10(d)); see Section 6 for discussion.

The zonal means of the moisture flux convergence and net precipitation are shown in Figure 11. Highest values, up to 110 mm per season, occur between 60 and 70°N, whereas minimum values occur between 70 and 80°N in every season except summer. In summer, the minimum values occur between 60 and 65°N, whereas maximum values occur from 75°N to the Pole. North of 72°N, the flux convergence peaks in summer and the net precipitation in summer or autumn. This is in agreement with analyses based on rawinsonde sounding data (Walsh *et al*., 1994).

In spring and summer, the flux convergence exceeds net precipitation almost everywhere, on average by 10.5 mm per season in spring and 7.1 mm per season in summer (Table II). The largest differences, up to 33 mm per season, occur in spring at 55–60 °N. In winter the difference is small, only 0.6 mm per season. In autumn, however, the zonal mean net precipitation exceeds the flux convergence, on average by 4.4 mm per season. As annual means north of 70 °N, the moisture flux convergence is 13 mm year^{-1} (7%) larger than the net precipitation. This demonstrates that, above all in spring and summer, the net effect of data assimilation in ERA-40 is to enhance moisture flux convergence.

The ERA-40 results for the spatial distribution of moisture flux convergence (Figure 10(a)) are qualitatively in agreement with those based on the NCEP1 reanalysis for 1970–1999 (Serreze and Barry, 2005): the maxima and minima are located in the same regions, and the magnitudes do not differ much. Regional differences can be found, but the agreement between the moisture flux convergences in ERA-40 and NCEP1 reanalyses is much better than the agreement between moisture flux convergence and net precipitation in NCEP1. The net precipitation is only 60% of the moisture flux convergence (Serreze and Barry, 2005), demonstrating that also in NCEP1 reanalysis the net effect of data assimilation is to enhance moisture flux convergence, but much more strongly than in ERA-40.

The IPWV and precipitation reach their maximum values in summer at 55–70°N. The flux convergence and net precipitation have, however, a summer minimum (in July even negative values) and peak in autumn (Figure 11 and Serreze *et al*., 2006). Serreze *et al*. (1995a, 1995b) explained this by strong cancellations between regions of strong pole-ward and equator-ward moisture fluxes in July. By contrast, although the fluxes are generally more modest in September, there is less compensation between regions of inflow and outflow.

The ratio of evaporation and moisture flux convergence shows the relative importance of the two source terms of moisture in the Arctic atmosphere. At most of the polar cap (70–90°N), from 72% of the area in autumn to 86% in winter, the ratio is less than 1. The ratio of spatially and seasonally averaged values is 0.93 in winter, 0.85 in

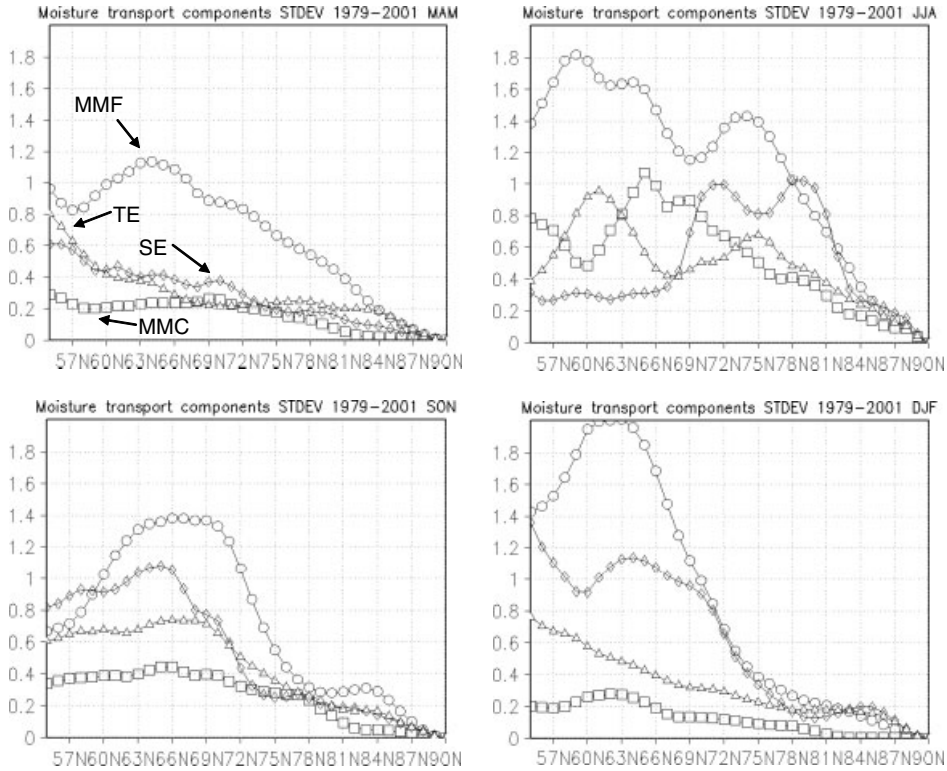

Figure 12. Inter-annual standard deviations of MMF, MMC, SE and TE in 1979–2001 for spring (MAM), summer (JJA), autumn (SON) and winter (DJF).

spring, 0.81 in autumn and 0.57 in summer. In winter, the ratio strongly depends on the surface type, being less than 0.1 over Greenland and the ice-covered Arctic Ocean, and more than 10 over the ice-free parts of the Greenland Sea and Norwegian Sea.

5. Inter-annual variations and large-scale circulation indices

The inter-annual variability in air temperature, evaporation, precipitation, net precipitation and IPWV is illustrated in Figure 1. The inter-annual STDs of the water vapour flux components are presented in Figure 12. The sum of the components, MMF, usually has the highest inter-annual variability. The inter-annual STD of SE transport is often higher than that of TE, even though TE averages are much higher. Averaged over latitudes 70–90 °N, in summer and winter the STD of SE transport is larger than that of TE transport (Table II), and for 55–69°N this is the case in autumn and winter. The inter-annual variation in MMC is usually smallest, but summer at lower latitudes is an exception: south of 57°N and from 64 to 69°N the STD of MMC exceeds those of SE and TE. For the annual means over 70–90 °N, the STD/mean ratio is highest for the SE transport (1.33), second highest for the MMC transport (0.61) and smallest for the TE transport (0.08). Over 55–69 °N, the order is: MMC (0.39), SE (0.12) and TE (0.04).

MMF inter-annual variability is higher in the Atlantic and North Pacific sectors with an inter-annual STD up to 15 kg m^{-1} s^{-1}. The inter-annual variability is smallest, less than 3 kg m^{-1} s^{-1}, in Greenland and the Hudson Bay. The TE variability is highest, up to 5 kg m^{-1} s^{-1}, in the Labrador Sea and Aleutians. The SE variability is highest, up to 6 kg m^{-1} s^{-1}, in the Norwegian Sea and Greenland. The STD/mean ratio is for TE from 0.1 to 0.5, except in areas near the North Pole, where the ratio exceeds 5, as the mean TE is very small (<1 kg m^{-1} s^{-1}). For MMF and SE, this ratio has a complex spatial distribution with maximum values more than 5 in numerous places.

On the basis of NCEP1 reanalysis, Sorteberg and Walsh (2008) stressed the importance of the variability in cyclone activity over the Greenland Sea and East Siberian Sea; these regions together account for 55% of the variability of the total moisture transport across 70 °N. Our results for the inter-annual STD of MMF suggest, however, that the most important regions are the Norwegian and Greenland Seas, the Bering Strait and, especially in summer, the sector between Barents and Laptev Seas. Sorteberg and Walsh (2008) concluded that during winter the variability in the dominant Greenland Sea cyclone activity alone accounts for 49% of the variability in the total moisture transport across 70°N by inducing strong variability in the Norwegian Sea moisture transport. This is in line with our result of a large inter-annual variability in the SE transport in winter: the variability is dominated by the region on the lee side of the Icelandic Low. On the other hand, in spring the inter-annual variability in moisture transport is significantly affected by seven cyclone regions (Sorteberg and Walsh, 2008). We interpret this so that the role of the large

Table III. Correlation coefficients between mean meridional moisture flux (MMF) and its components (MMC, SE, TE), precipitable water (IPWV) and net precipitation ($P - E$) over the polar cap (70–90 °N) and the seasonal NAO and AO indices for years 1979–2001.

	MAM		JJA		SON		DJF		Year	
	NAO	AO	NAO	AO	NAO	AO	NAO	AO	NAO	AO
MMF	0.39	**0.53**	0.34	**0.79**	0.22	0.22	**0.45**	**0.52**	**0.49**	**0.62**
MMC	0.13	0.30	0.31	**0.47**	0.23	0.39	−0.01	0.17	0.40	**0.45**
SE	**0.46**	0.43	−0.23	0.00	0.38	−0.20	**0.51**	0.41	0.41	0.24
TE	0.17	**0.52**	**0.52**	**0.83**	−0.26	0.14	−0.02	0.11	0.07	0.29
IPWV	−0.04	0.09	−0.01	0.13	0.04	**−0.61**	0.14	−0.20	−0.03	−0.08
$P - E$	0.43	**0.56**	0.33	**0.69**	0.11	0.14	0.30	0.36	0.39	**0.47**

Statistically significant (95%) correlations are marked in bold.

standing eddies is less dominant, which is related to a relatively small STD of SE transport in spring compared with other seasons (Figure 12).

There is a well-known relationship between the atmospheric moisture budget and the large-scale atmospheric circulation, as characterized by the AO and NAO indices (Dickson *et al*., 2000; Boer *et al*., 2001; Rogers *et al*., 2001; Oshima and Yamazaki, 2004). NAO and AO are nearly indistinguishable in the time domain: the correlation coefficient (r) of monthly anomalies over the Northern Hemisphere in November–April is 0.95 (Dickson *et al*., 2000). The signature of AO on local temperatures and precipitation is therefore essentially the same as that of NAO. We found, however, that for the areally averaged variables, the correlations are higher with the AO than NAO index (Table III). Hence, we focus our analyses to the AO index.

In ERA-40, averaged over the polar cap, MMF had a significant positive correlation with AO at every season except autumn; in summer it reached $r = 0.79$. This is noteworthy, as the effects of AO are usually most apparent in winter and spring (Serreze and Barry, 2005). There was significant negative correlation ($r = -0.61$) between IPWV and AO in autumn. The net precipitation had a significant positive correlation with AO in summer ($r = 0.69$) and spring ($r = 0.56$).

Geographical distributions of the seasonal correlations of MMF, SE, IPWV and $P - E$ with AO for years 1979–2001 are shown in Figure 13. In every season, especially in winter, there is a region of a significant positive correlation between MMF and AO in the Norwegian and Barents Seas. Large areas of significant correlation between the SE transport and AO can be found in all seasons except autumn. In summer, the correlations over the North America are clearly stronger than over Eurasia. In winter, strong correlations are found also over the Norwegian Sea. These are related to high correlations between AO (and NAO) and several cyclone-related variables: intensity, track density, speed, growth/decay rate and lifetime (Sorteberg *et al*., 2005).

In winter the IPWV and AO correlate negatively in Canada and Greenland but positively in Europe. In spring, the principal region of a positive correlation moves to western Siberia. Except of very small regions, in autumn the only significant correlations are negative ones, whereas positive in summer. In winter, the correlation between net precipitation and AO is positive in the Norwegian and Iceland Seas. In summer, significant positive correlations can be found mostly over the sea and negative ones over the land. In all seasons, AO correlates similarly with net precipitation and precipitation, but differently with evaporation. In autumn, the influences of large-scale circulation indices are often weaker (Jaagus, 2006), which is also seen from Figure 13.

6. Discussion

Comparing the moisture flux convergence and net precipitation, the former is a true analysis quantity, i.e. it depends on the first-guess field and assimilation of observations of the air moisture and wind, as well as quantities affecting the wind and moisture analyses, such as the air pressure and temperature. The precipitation and evaporation fields in ERA-40 and other reanalyses are, however, solely based on short-term forecasts. If the difference between moisture flux convergence and net precipitation is small, the reanalysis is close to a hydrological balance, i.e. the data assimilation does not have a net effect of enhancing or decreasing the moisture flux convergence. Considering the annual mean north of 55 °N, the moisture flux convergence is 277 mm year^{-1} and the net precipitation is 252 mm year^{-1}, whereas the respective numbers are 192 and 179 mm year^{-1} for the region north of 70 °N. The relative differences are 10% (55–90 °N) and 7% (70–90 °N). This demonstrates that in the Arctic and northern mid-latitudes the net effect of data assimilation in ERA-40 is to enhance moisture flux convergence, above all in spring and summer, by either adding moisture to the first-guess field or modifying the wind field. Enhanced moisture flux convergence results, however, in enhanced removal of moisture from the model atmosphere. It is noteworthy that the relative differences between net precipitation and flux convergence are smaller in the Antarctic: 3% over the Southern Ocean and 5% over the continental ice sheet (Tietäväinen

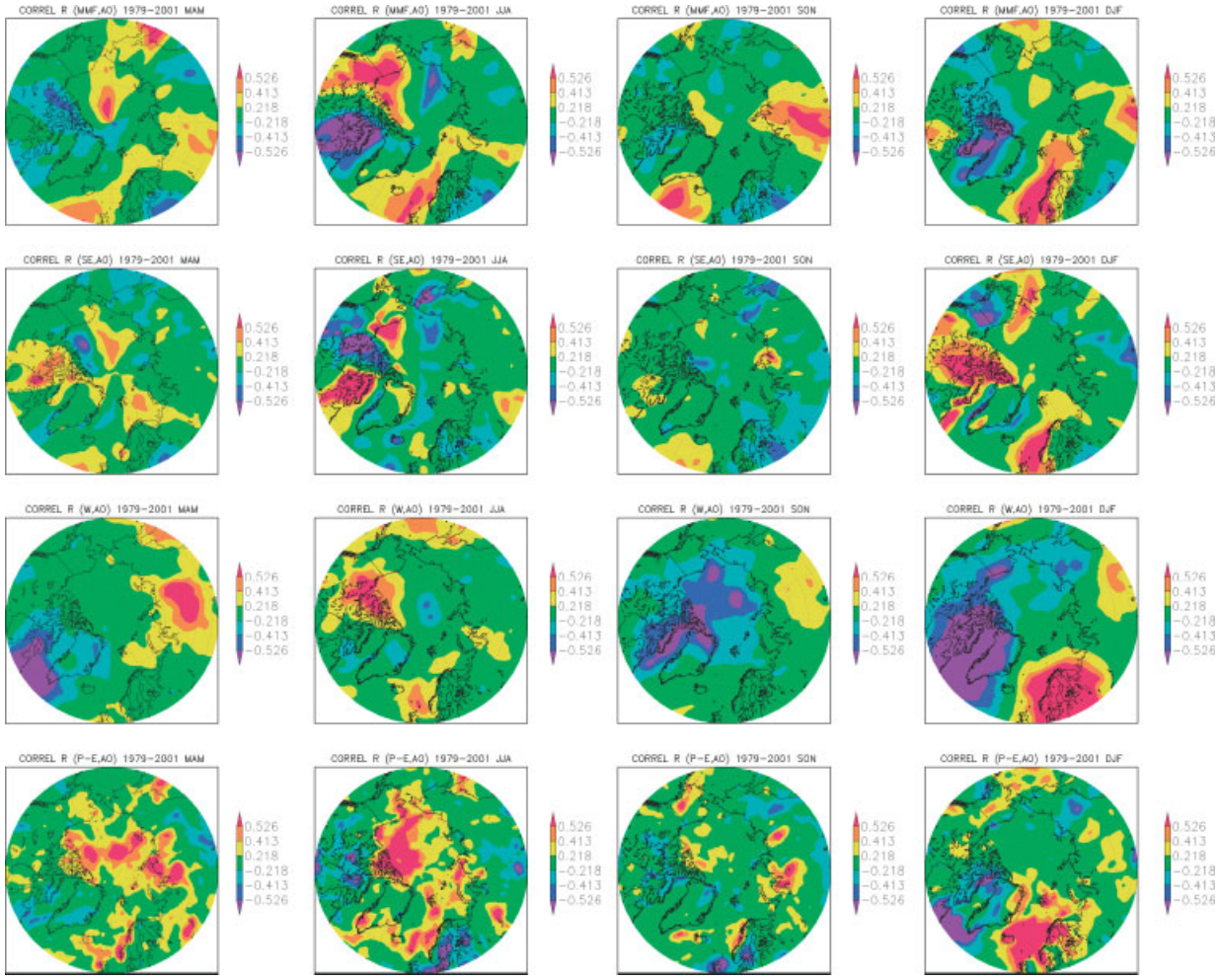

Figure 13. Seasonal correlations of MMF, SE, IPWV and $P - E$ with AO for years 1979–2001. The colour codes correspond to 68% ($|r| > 0.218$), 95% ($|r| > 0.413$) and 99% ($|r| > 0.526$) confidence levels. This figure is available in colour online at wileyonlinelibrary.com/journal/joc

and Vihma, 2008). This probably results from the simpler topography.

Excluding the topographic effects, the relative differences between the net precipitation and water vapour flux convergence did not show strong dependence on the latitude (Figure 10(d)). This is also seen in the above-mentioned area-averaged relative differences (7% and 10%). This does not, however, mean that the model products for the air humidity are as good in the Arctic as in lower latitudes. The difference between the moisture flux convergence and net precipitation is often used as a measure of the quality of model analyses and reanalyses (Bromwich *et al*., 2002; Simmons *et al*., 2007). A good hydrological balance requires good schemes for moisture advection, cloud physics, precipitation and evaporation, and there has been an improvement in the hydrological balance from ERA-15 to ERA-40 (Bromwich *et al*., 2002) and further to ERA-Interim (Simmons *et al*., 2007). A good hydrological balance is, however, also achieved, if a few moisture data are assimilated into the reanalysis. The moisture data assimilation is very limited in the snow/ice-covered regions in the Arctic, and we regard this as an important fact to explain our observation that the relative differences between the net precipitation and flux convergence are not larger in the Arctic than at lower latitudes.

The relative accuracy of net precipitation and flux convergence depend on the season and geographic region (Tietäväinen and Vihma, 2008). Over the open ocean, the model analysis for both specific humidity and wind strongly benefit from the assimilation of remote sensing data (Uppala *et al*., 2005), whereas the accuracy of the evaporation parameterized by the bulk method is probably no better than ±20% (Cronin *et al*., 2006), and sometimes even much worse (Cullather *et al*., 2000). Cullather *et al*. (2000) concluded that the moisture flux convergence is much more realistic than the forecast values for net precipitation, with the major source of the hydrologic imbalance being the forecasted evaporation. Over the open ocean, these aspects favour the accuracy of the water vapour flux convergence. Over sea ice and snow-covered land, however, the absolute error in the small evaporation is much less than over the open ocean. Furthermore, the reanalysis does not benefit from remote sensing information on specific humidity and scatterometer winds, and rawinsonde data are seldom available from

the Arctic Ocean. The assimilation of pressure and temperature data does, however, influence the wind field, and therefore also the analysis of moisture flux convergence, generating a difference between the flux convergence and net precipitation also over snow/ice-covered surfaces. Serreze *et al*. (2006) consider the ERA-40 water vapour flux convergence more reliable than the net precipitation based on 6-h forecasts. We agree on this at least over the open ocean. This may have implications for the choice of the best upper boundary conditions for the freshwater flux in ocean models applied in climate simulations.

7. Conclusions

The key new findings of this study are summarized below.

1. Previous studies based on coarse-resolution rawinsonde data have suggested that the northward moisture transport across 70°N peaks is at the 850-hPa pressure level (Overland and Turet, 1994; Serreze *et al*., 1995a, 1995b). According to ERA-40, however, the peak MMF usually occurs below the 900-hPa pressure level; this is the case for 94% of the data in autumn, 87% in spring, 77% in summer and 63% in winter. The median peak level is in winter at 930 hPa pressure level and in other seasons at 970–990 hPa level. Another clear difference between results based on rawinsonde and ERA-40 data is that according to the former the mean v wind at 70°N is southward up to 400 hPa level (Serreze *et al*., 1995b), whereas in ERA-40 it is southward only up to 950 hPa level.
2. Results on moisture transport to the polar cap based on different datasets (rawinsondes, NCEP/NCAR reanalysis and ERA-40) agree within 2% in every season, but the differences are larger, 5–8%, in the moisture flux convergence and net precipitation. The agreement between NCEP/NCAR and ERA-40 in the flux convergence is, however, much better than the agreement between the flux convergence and net precipitation within NCEP/NCAR.
3. In previous studies, the moisture transport has been divided into the contributions of MMC and eddy activity, usually without separation of SE and TE, and the cyclone activity at 70°N has been argued to be a good predictor for both seasonal and inter-annual moisture transport variability (Sorteberg and Walsh, 2008). So far, however, the importance of the cyclone activity on the inter-annual variability in moisture transport was not quantified. We showed that the inter-annual variability is larger for SE and TE than for MMC in autumn, winter and spring. Furthermore, although SE represents only 4% of TE north of 70°N, the inter-annual variability is particularly large for SE in summer and winter. The SE inter-annual variability (0.66 and 0.53 kg m^{-1} s^{-1} in summer and winter, respectively) is the main contributor to the variability in the total moisture transport (0.94 and 0.59 kg m^{-1} s^{-1} in summer and winter), exceeding the variability of TE (0.59 and 0.42 kg m^{-1} s^{-1} in summer and winter). As an annual mean, the STD/mean ratio is 1.33 for SE and 0.08 for TE.
4. The spatial distributions of net precipitation and moisture flux convergence are qualitatively similar. The absolute difference field includes, however, values with magnitudes exceeding 200 mm $year^{-1}$. Due to the numerical methods applied, large differences occur over areas with much topographic variations. A larger flux convergence is common in sea areas with a high cyclonic activity, such as the Norwegian and Iceland Seas and the Gulf of Alaska, whereas a larger net precipitation is typical for the neighbouring land areas. Seasonally, the discrepancy between the flux convergence and net precipitation is largest in spring and summer.
5. The area averages of ERA-40 based MMF and $P - E$ had higher correlations with the AO than NAO at every season, although Rogers *et al*. (2001) had found for the Arctic Basin that annual $P - E$ in NCEP/NCAR reanalysis is much more closely correlated with the NAO ($r = 0.69$) than the AO ($r = 0.49$). In ERA-40, the highest correlations with AO were observed for MMF in spring and winter ($r = 0.75$), and for the net precipitation in spring ($r = 0.61$) and winter ($r = 0.50$). Although there were no significant correlations between AO and the area-averaged IPWV, there was a high negative correlation in Canada and Greenland in winter and spring ($r = 0.7$), and a positive correlation in Europe in winter ($r = 0.8$).

Further improvement of atmospheric moisture budget in Arctic reanalyses is expected to come from (1) better model resolution allowing better detection of mesoscale cyclones, (2) application of four-dimensional variational data assimilation (as in ERA-Interim) and (3) assimilation of satellite-based moisture data over snow/ice-covered regions (Melsheimer and Heygster, 2008). Considering the future Arctic climate under increasing atmospheric greenhouse gas concentrations, the importance of SE is not expected to decrease. A common signal in 14 out of the 16 global climate model simulations analysed by Brandefelt and Körnich (2008) was an unchanged or increased stationary wave amplitude.

Acknowledgements

This study was supported by the EU project DAMOCLES, which is financed in the 6th Framework Programme for Research and Development (grant 18 509), by DFG (grant LU 818/1-1), and by the Estonian Science Foundation (grant No. 7347). The ECMWF is acknowledged for data supply.

References

Aoki T, Aoki T, Fukabori M, Uchiyama A. 1999. Numerical simulation of the atmospheric effects on snow albedo with a multiple

scattering radiative transfer model for the atmosphere-snow system. *Journal of the Meteorological Society of Japan* **77**: 595–614.

Betts AK, Ball JH, Viterbo P. 2003. Evaluation of the ERA-40 surface water budget and surface temperature for the Mackenzie river basin. *Journal of Hydrometeorology* **4**: 1194–1211.

Boer GJ, Fourest S, Yu B. 2001. The signature of the annular modes in the moisture budget. *Journal of Climate* **14**: 3655–3665.

Box JE, Bromwich DH, Veenhuis BA, Bai LS, Stroeve JC, Rogers JC, Steffen K, Haran T, Wang SH. 2006. Greenland ice sheet surface mass balance variability (1988–2004) from calibrated polar MM5 output. *Journal of Climate* **19**: 2783–2800.

Brandfelt J, Körnich H. 2008. Northern hemisphere stationary waves in future climate projections. *Journal of Climate* **21**: 6341–6353.

Bromwich DH, Fogt RL, Hodges KI, Walsh JE. 2007. A tropospheric assessment of the ERA-40, NCEP, and JRA-25 global reanalyses in the polar regions. *Journal of Geophysical Research* **112**: D101111–D1011121, DOI:10.1029/2006JD007859.

Bromwich DH, Wang S-H. 2005. Evaluation of the NCEP-NCAR and ECMWF 15- and 40-yr reanalyses using rawinsonde data from two independent Arctic field experiments. *Monthly Weather Review* **133**: 3562–3578.

Bromwich DH, Wang S-H. 2008. A review of the temporal and spatial variability of Arctic and Antarctic atmospheric circulation based upon ERA-40. *Dynamics of Atmospheres and Oceans* **44**: 213–243, DOI:10.1016/j.dynatmoce.2007.09.001.

Bromwich DH, Wang S-H, Monaghan AJ. 2002. *ERA-40 representation of the Arctic atmospheric moisture budget*, ERA-40 Project Report Series 3. ECMWF: Reading.

Calanca P, Fortelius C. 1996. Representation of model data and evaluation of diagnostic equations in pressure coordinates. *Tellus* **48A**: 756–766.

Cheng B, Zhang Z, Vihma T, Johansson M, Bian L, Li Z, Wu H. 2008. Model experiments on snow and ice thermodynamics in the Arctic Ocean with CHINARE 2003 data. *Journal of Geophysical Research* **113**: C09020, DOI:10.1029/2007JC004654.

Condron A, Bigg GR, Renfrew IA. 2006. Polar mesoscale cyclones in the northeast Atlantic: comparing climatologies from ERA-40 and satellite imagery. *Monthly Weather Review* **134**: 1518–1533.

Cronin MF, Fairall CW, McPhaden MJ. 2006. An assessment of buoy derived and numerical weather prediction surface heat fluxes in the tropical Pacific. *Journal of Geophysical Research* **111**: C06038, DOI:10.1029/2005JC003324.

Cullather RI, Bromwich DH, Serreze MC. 2000. The atmospheric hydrologic cycle over the Arctic basin from reanalyses. Part I: comparison with observations and previous studies. *Journal of Climate* **13**: 923–937.

Curry JA, Rossow WB, Randall D, Schramm JL. 1996. Overview of Arctic cloud and radiation characteristics. *Journal of Climate* **9**: 1731–1764.

Dickson RR, Meincke J, Vassie IM, Junclaus J, Osterhus S. 1996. Long-term coordinated changes in the convective activity of the North Atlantic. *Progress in Oceanography* **38**: 241–295.

Dickson RR, Osborn TJ, Hurrell JW, Meincke J, Blindheim J, Adlandsvik B, Vinje T, Alekseev G, Maslowski W. 2000. The Arctic Ocean response to the North Atlantic oscillation. *Journal of Climate* **13**: 2671–2696.

Fiorino M. 2004. *A Multi-decadal Daily Sea Surface Temperature and Sea Ice Concentration Data Set for the ERA-40 Reanalysis*, ERA-40 Project Report Series 12. ECMWF: Reading.

Gober M, Hagenbrock P, Ament F, Hense A. 2003. Comparing mass-consistent atmospheric moisture budgets on an irregular grid: An Arctic example. *The Quarterly Journal of the Royal Meteorological Society* **129**: 2383–2400.

Granskog M, Vihma T, Pirazzini R, Cheng B. 2006. Superimposed ice formation and surface fluxes on sea ice during the spring melt-freeze period in the Baltic Sea. *Journal of Glaciology* **52**: 119–127.

Groves DG, Francis JA. 2002. Variability of the Arctic atmospheric moisture budget from TOVS satellite data. *Journals of Geophysical Research-Atmospheres* **107**(D24): DOI: 10.1029/2002JD002285.

Intrieri JM, Fairall CW, Shupe MD, Persson POG, Andreas EL, Guest PS, Moritz RE. 2002. An annual cycle of Arctic surface cloud forcing at SHEBA. *Journal of Geophysical Research* **107**: 8039, DOI: 10.1029/2000JC000439.

Jaagus J. 2006. Trends in sea ice conditions on the Baltic Sea near the Estonian coast during the period 1949/50–2003/04 and their relationships to large-scale atmospheric circulation. *Boreal Environment Research* **11**: 169–183.

Kaleschke L, Lüpkes C, Vihma T, Haarpaintner J, Bochert A, Hartmann J, Heygster G. 2001. SSM/I sea ice remote sensing for mesoscale ocean-atmosphere interaction analysis. *Canadian Journal of Remote Sensing* **27**: 526–536.

Kållberg P, Berrisford P, Hoskins B, Simmons A, Uppala S, Lamy-Thépaut S, Hine R. 2005. *ERA-40 Atlas*, ERA-40 Project Report Series 19. ECMWF: Reading.

Melsheimer C, Heygster G. 2008. Improved retrieval of total water vapor over polar regions from AMSU-B microwave radiometer data. *IEEE Transactions on Geoscience and Remote Sensing* **46**: 2308–2322, DOI:10.1109/TGRS.2008.918013.

Oshima K, Yamazaki K. 2004. Seasonal variation of moisture transport in polar regions and the relation with annular modes. *Polar Meteorology and Glaciology* **18**: 30–53.

Oshima K, Yamazaki K. 2006. Difference in seasonal variation of net precipitation between the Arctic and Antarctic regions. *Geographical Research Letters* **33**: 1–4, DOI:10.1029/2006GL027389.

Overland JE, Turet P. 1994. Variability of the atmospheric energy flux across 70 °N computed from the GFDL data set. In: *The Polar Oceans and Their Role in Shaping the Global Environment*, *Geophysical Monograph Series 85*, Johannessen OM, Muench RD, Overland JE (eds). American Geophysical Union: Washington, DC.

Palmen E, Vuorela LA. 1963. On the mean meridional circulationsin the Northern Hemisphere during the winter season. *Quarterly Journal of the Royal Meteorological Society* **89**: 131–138.

Peixoto JP, Oort AH. 1983. The atmospheric branch of the hydrological cycle and climate. In *Variations in the Global Water Budget*. Reidel Publishing Co: Norwell.

Peixoto JP, Oort AH. 1992. *Physics of Climate*. American Institute of Physics: New York.

Prata AJ. 1996. A new longwave formula for estimating downward clear-sky radiation at the surface. *The Quarterly Journal of the Royal Meteorological Society* **122**: 1127–1151.

Rasmussen EA, Turner J. 2003. *Polar Lows: Mesoscale Weather Systems in the Polar Regions*. Cambridge University Press: Cambridge.

Rinke A, Melsheimer C, Dethloff K, Heygster G. 2008. Arctic total water vapor: comparison of regional climate simulations with observations, and simulated decadal trends. *Journal of Hydrometeorology* DOI: 10.1175/2008JHM970.1.

Rogers AN, Bromwich DH, Sinclair EN, Cullather RI. 2001. The atmospheric hydrologic cycle over the Arctic basin from reanalyses. Part II: inter annual variability. *Journal of Climate* **14**: 2414–2429.

Sellers WD. 1965. *Physical Climatology*. University of Chicago Press: Chicago.

Serreze MC, Barrett A, Lo F. 2005. Northern high latitude precipitation as depicted by atmospheric reanalyses and satellite retrievals. *Monthly Weather Review* **133**: 3407–3430.

Serreze MC, Barrett AP, Slater AG, Steele M, Zhang J, Trenberth KE. 2007. The large-scale energy budget of the Arctic. *Journal of Geophysical Research* **112**: D11122, DOI: 10.1029/2006JD008230.

Serreze MC, Barrett AP, Slater AG, Woodgate RA, Aagaard K, Lammers RB, Steele M, Moritz R, Meredith M, Lee CM. 2006. The large-scale freshwater cycle of the Arctic. *Journal of Geophysical Research* **111**(C11): DOI:10.1029/2005JC003424.

Serreze MC, Barry RG. 2000. Atmospheric components of the Arctic Ocean hydrologic budget assessed from rawinsonde data. In *The Freshwater Budget of the Arctic Ocean*, Lewis EL, Jones EP, Lemke P, Prowse TD, Wadhams P (eds). Kluwer Academic Press: Dordrecht.

Serreze MC, Barry RG. 2005. *The Arctic Climate System*. Cambridge University Press: Cambridge.

Serreze MC, Barry RG, Rehder MC, Walsh JE, Drewry D. 1995a. Variability in atmospheric circulation and moisture flux over the Arctic. *Philosophical Transactions: Physical Sciences and Engineering* **352**: 215–225.

Serreze MC, Barry RG, Walsh JE. 1995b. Atmospheric water vapour characteristics at 70 °N. *Journal of Climate* **8**: 719–731.

Serreze MC, Etringer AJ. 2003. Precipitation characteristics of the Eurasian Arctic drainage system. *International Journal of Climatology* **23**: 1267–1291.

Simmons AJ, Hollingsworth A. 2002. Some aspects of the improvement in skill of numerical weather prediction. *Quarterly Journal of the Royal Meteorological Society* **128**: 647–677.

Simmons AJ, Uppala S, Dee D, Kobayashi S. 2007. *ERA–Interim: New ECMWF Reanalysis Products from 1989 Onwards*, Newsletter 110. ECMWF: Reading.

Sorteberg A, Katsov V, Walsh J, Palova T. 2007. The Arctic surface energy budget as simulated with the IPCC AR4 AOGCMs. *Climate Dynamics* **29**: 131–156, DOI: 10.1007/s00382-006-0222-9.

Sorteberg A, Kvamstø NG, Byrkjedal O. 2005. Wintertime Nordic Seas cyclone variability and its impact on oceanic volume transport into the Nordic Seas. In *The Nordic Seas: An Integrated Perspective*, *AGU Geophysical Monograph Series 158*, Drange H (ed). American Geophysical Union: Washington.

Sorteberg A, Walsh JE. 2008. Seasonal cyclone variability at 70 °N and its impact on moisture transport into the Arctic. *Tellus* **60A**: 570–586, DOI:10.1111/j.1600-0870.2008.00314.x.

Tietäväinen H, Vihma T. 2008. Atmospheric moisture budget over Antarctica and the Southern Ocean based on the ERA-40 reanalysis. *International Journal of Climatology* DOI: 10.1002/joc.1684.

Trenberth KE, Fasullo J, Smith L. 2005. Trends and variability in column-integrated atmospheric water vapor. *Climate Dynamics* **24**: 741–758, DOI: 10.1007/s00382-005-0017-4.

Trenberth KE, Smith L. 2006. The vertical structure of temperature in the tropics: different flavours of El Nino. *Journal of Climate* **19**: 4956–4973.

Uppala SM, Kållberg PW, Simmons AJ, Andrae U, da Costa Bechtold V, Fiorino M, Gibson JK, Haseler J, Hernandez A, Kelly GA, Li X, Onogi K, Saarinen S, Sokka N, Allan RP, Andersson E, Arpe K, Balmaseda MA, Beljaars ACM, van de Berg L, Bidlot J, Bormann N, Caires S, Chevallier F, Dethof A, Dragosavac M, Fisher M, Fuentes M, Hagemann S, Hólm E, Hoskins BJ, Isaksen L, Janssen PAEM, Jenne R, McNally AP, Mahfouf J-F, Morcrette J-J, Rayner NA, Saunders RW, Simon P, Sterl A, Trenberth KE, Untch A, Vasiljevic D, Viterbo P, Woollen J. 2005. The ERA-40 re-analysis. *Quarterly Journal of the Royal Meteorological Society* **131**: 2961–3012, DOI: 10.1256/qj.04.176.

Valkonen T, Vihma T, Doble M. 2008. Mesoscale modelling of the atmospheric boundary layer over the Antarctic sea ice: a late autumn case study. *Monthly Weather Review* **136**: 1457–1474.

Vihma T, Lüpkes C, Hartmann J, Savijärvi H. 2005. Observations and modelling of cold-air advection over Arctic sea ice in winter. *Boundary-Layer Meteorology* **117**: 275–300.

Walsh JE, Zhou X, Portis D, Serrese MC. 1994. Atmospheric Contribution to Hydrologic Variations in the Arctic. *Atmosphere-Ocean* **32**(4): 733–755.

White D, Hinzman L, Alessa L, Cassano J, Chambers M, Falkner K, Francis J, Gutowski WJ Jr., Holland M, Holmes RM, Huntington H, Kane D, Kliskey A, Lee C, McClelland J, Peterson B, Rupp TS, Straneo F, Steele M, Woodgate R, Yang D, Yoshikawa K, Zhan T. 2007. The arctic freshwater system: changes and impacts. *Journal of Geophysical Research* **112**: G04S54, DOI:10.1029/2006JG000353.

Zhang X, Walsh JE, Zhang J, Bhatt US, Ikeda M. 2004. Climatology and interannual variability of Arctic cyclone activity: 1948–2002. *Journal of Climate* **17**: 2300–2317.

